Basin Research (2001) **13,** 335–357

Causes of spatially variable tectonic subsidence in the Miocene Bermejo Foreland Basin, Argentina

N. Cardozo and T. Jordan

Department of Earth and Atmospheric Sciences, Snee Hall, Cornell University, Ithaca, NY 14853–1504, USA (nfc3@cornell.edu, tej1@cornell.edu)

ABSTRACT

Tectonic subsidence in the 20–9 Ma Bermejo basin resulted from spatially variable crustal loading on a lithosphere of spatially variable strength (e.g. elastic thickness). Reconstruction of the crustal loads added between 20 and 9 Ma, and assessment of the effects of these loads on an elastic, isotropic lithosphere confirm this hypothesis. Elastic models effectively explain tectonic subsidence east of the Iglesia–Calingasta basin, but west of it crustal loads were locally compensated. Elastic models also prove that the 20–9 Ma Frontal Cordillera loading is of no importance in the mechanical system of the Bermejo basin. 2D and 3D elastic models of a uniformly strong lithosphere under 20–9 Ma crustal loads corrected for post-9 Ma erosion successfully replicate the 9 Ma Bermejo basin's proximal palaeotopography. However, they fail to replicate the 9 Ma basin's medial and distal palaeotopography. A 3D finite element model of a lithosphere with bimodal strength (weak below the Bermejo basin and west of the Precordillera, and strong below the Precordillera and east of the Valle Fértil lineament) successfully replicates the 9 Ma basin's palaeotopography. That variable strength model introduces a southward decrease in the wavelength of flexural deformation, which results in a basin that narrows southward, consistent with the 9 Ma Bermejo basin. The preferred 9 Ma lithospheric strength distribution is similar to the present lithospheric strength field derived from gravity data, suggesting that the bimodal strength signature was retained throughout the entire basin's evolution. Late Miocene flattening of the subducting slab, tectonic change to a broken foreland, or deposition of a thick (~8–10 km) sedimentary cover did not affect the strength of the lithosphere underlying the Bermejo basin. The long-term bimodal strength field does not correlate with the documented thickness of the seismogenic crust.

INTRODUCTION

In an ideal foreland basin, crustal loads, tectonic subsidence and the basin's cross-sectional geometry are constant along strike (Flemings & Jordan, 1989). But in nature, spatially and temporally variable tectonic shortening (Whiting & Thomas, 1994; DeCelles & Mitra, 1995), exhumation (Flemings & Nelson, 1991; Schlunegger, 1999), climate and/or sediment supply (Horton, 1999) create crustal loads that are variable both in space and time. These loads are imposed on a basin's underlying lithosphere that may also have spatially and even temporally variable strength (Beaumont, 1981; Watts, 1992; Clark & Royden, 2000), resulting in tectonic subsidence and stratal geometries that are variable in space and time.

The Miocene Bermejo basin in the Argentine Andean foreland is no exception. Based on isopach maps of the basin, Jordan *et al*. (2001) hypothesized that spatial and temporal variability of both crustal loads and mechanical behaviour of the lithosphere resulted in a basin geometry that varied along strike. However, the details of the mechanisms that caused tectonic subsidence in the basin and the effects of spatially variable loads and lithospheric strength were not entirely understood. Spatial variability of lithospheric strength in the present Andean foreland has been extensively investigated with gravity data (Yañez *et al*., 1995; Giménez, 1997; Stewart & Watts, 1997), but the strength of the lithosphere in ancient situations and the evolution of its mechanical state have been largely ignored.

In this paper, we evaluate the effects of spatially variable crustal loads and lithospheric strength on the tectonic subsidence of the Bermejo basin during its Miocene 'simple foreland' stage (Jordan *et al*., 2001). Based on an accurate but imprecise chronology of thrust motion (~1–10 Myr uncertainties) and a more precise chronology of basin filling (~0.1–1 Myr uncertainties), we

reconstruct the crustal loads added during the evolution of the Miocene basin. Explicitly in this process, we assume that erosion lowered the upper envelope of the tectonic loads to a regional, critical slope. We then evaluate the lithospheric deformation caused by these crustal loads using 2D and 3D elastic models. Our results suggest that the geometry of the Miocene Bermejo strata and palaeogeography of the late Miocene basin are explained by spatially variable crustal loads and lithospheric strength, and also by a lithospheric strength distribution that is temporally steady and retained over long times.

GEOLOGICAL SETTING

The Bermejo basin

The Bermejo Valley of north-western Argentina (29–32°S, 67–69°W) is bounded on the west by the Precordillera fold–thrust belt, and on the east by the reverse fault-bounded crystalline basement uplifts of the Sierras Pampeanas (Fig. 1A,B). The Bermejo basin initiated 20 million years ago (Ma), and evolved during the early and middle Miocene beside a tectonically thickened mountain belt (the Precordillera thin-skinned thrust belt and the Frontal Cordillera hinterland) overlying a normally (30°) subducting slab (Kay *et al*., 1988; Jordan *et al*., 2001). This 'simple foreland' stage was modified in the late Miocene, when flattening of the slab (Kay *et al*., 1988) and reverse thick-skinned faulting in the Sierras Pampeanas (Jordan & Allmendinger, 1986), created multiple, separate, fault-bounded subbasins (Jordan *et al*., 2001). Today, the Bermejo basin is actively accumulating sediments adjacent to the zones of crustal thickening.

The 20–9 Ma Bermejo basin evolved during the most active stages of crustal shortening and thickening of the adjacent Frontal Cordillera and Precordillera, and before the onset of deformation of the Sierras Pampeanas (Jordan *et al*., 2001). The 20–9 Ma Bermejo basin strata thicken monotonically toward the west (except in the westernmost sites, where preserved sections are erosional remnants of sections whose thickness at 9 Ma is unknown, Fig. 2A,B). This wedge-like across-strike geometry suggests that tectonic subsidence in the basin is directly linked to crustal shortening and thickening in the adjacent mountain belt. Along strike, the sediments are thickest adjacent to the northern Precordillera and thin southward in the medial and distal parts of the basin (Fig. 2A,B). The basin narrows southward (Milana, 1991; Bercowski *et al*., 1994), from roughly 200 km near 30°S to perhaps only 100 km near 31°S (Fig. 2B). This north to south variability in stratal thicknesses implies along-strike variability in tectonically driven thickening in the Precordillera and/or Cordillera Frontal, and/or lithospheric strength, and/or sediment supply (Jordan *et al*., 2001).

The 20–9 Ma depositional environment configurations of the Bermejo basin are characterized by two facies motifs (Fig. 3, Jordan *et al*., 2001). In the first motif (Fig. 3A,C) proximal bajadas yielded eastward to aeolian dune fields (Cevallos & Milana, 1992; Jordan *et al*., 1993b; Milana *et al*., 1993; Milana, 1993). In distal positions further east, muddy very low-relief flats were transitional to dry lakes, which precipitated gypsum (Fig. 3C, Malizia *et al*., 1995). In the second motif (Fig. 3B,D,E) laterally extensive bajadas and local alluvial fans along the western flank of the basin graded eastward to lower surface gradients and finer grained sandy and muddy fluvial sediments. A broad lowland aligned parallel to the thrust belt collected muddy deposits (Fig. 3D,E). The muddy axis was a true regional topographic low, to the east of which surface elevations increased slightly toward an eastern source area (Malizia *et al*., 1995).

The facies motifs suggest that a topographic low persisted in the basin during its 20–9 Ma simple foreland stage. At early stages the topographic low is indicated by closed saline flats (Fig. 3B,C), and later by mudflats at the junction of west-derived strata with east-derived strata at Río Mañero (RM, Fig. 3D,E, Malizia *et al*., 1995). The depositional environment configurations imply that the 20–9 Ma Bermejo basin did not overfill its accommodation space to a large degree. If it had done so, rivers would have passed eastward across an entirely buried forebulge (Jordan, 1995; Jordan *et al*., 2001). The distance between the thrust front and the topographic low decreased through time, from about 250 km between 20 and 14 Ma (Fig. 3B,C), to about 150 km by 9 Ma (Fig. 3E).

The Precordillera thrust belt and the Frontal Cordillera

Accumulation of the 20–9 Ma Bermejo basin strata was contemporaneous with crustal shortening and thickening in the adjacent Western and Central Precordillera and nearby Frontal Cordillera (Jordan *et al*., 1993a). Therefore, flexure of the lithosphere beside a structurally thickened mountain belt (Jordan, 1981, 1995) was probably a primary cause of tectonic subsidence in the Bermejo basin. This relation applies from 29°S to 33°S; north and south of these latitudes the Precordillera morphostructural unit disappears.

The across-strike geometry of the Western and Central Precordillera (Allmendinger *et al*., 1990; von Gosen, 1992, 1995, 1997; Caminos *et al*., 1993; Ramos & Cristallini, 1995; Ramos *et al*., 1997) approximates a westward-thickening structural wedge, formed by eastward tectonic transport of Palaeozoic and locally Mesozoic strata (Fig. 4). Spatial variability in the distribution of the Palaeozoic and Mesozoic basins (Astini, 1991; Salfity & Gorustovich, 1983; Fernández-Seveso *et al*., 1993) imparts moderate along-strike variability in the thrust geometry (von Gosen, 1992, 1995, 1997). Nevertheless, the total shortening in the thrust belt is estimated to have been 70% on all cross-sections between 29°30′ and 31°30′S (Fig. 4). A significant along-strike difference, however, is that the depth to the decollement varies from

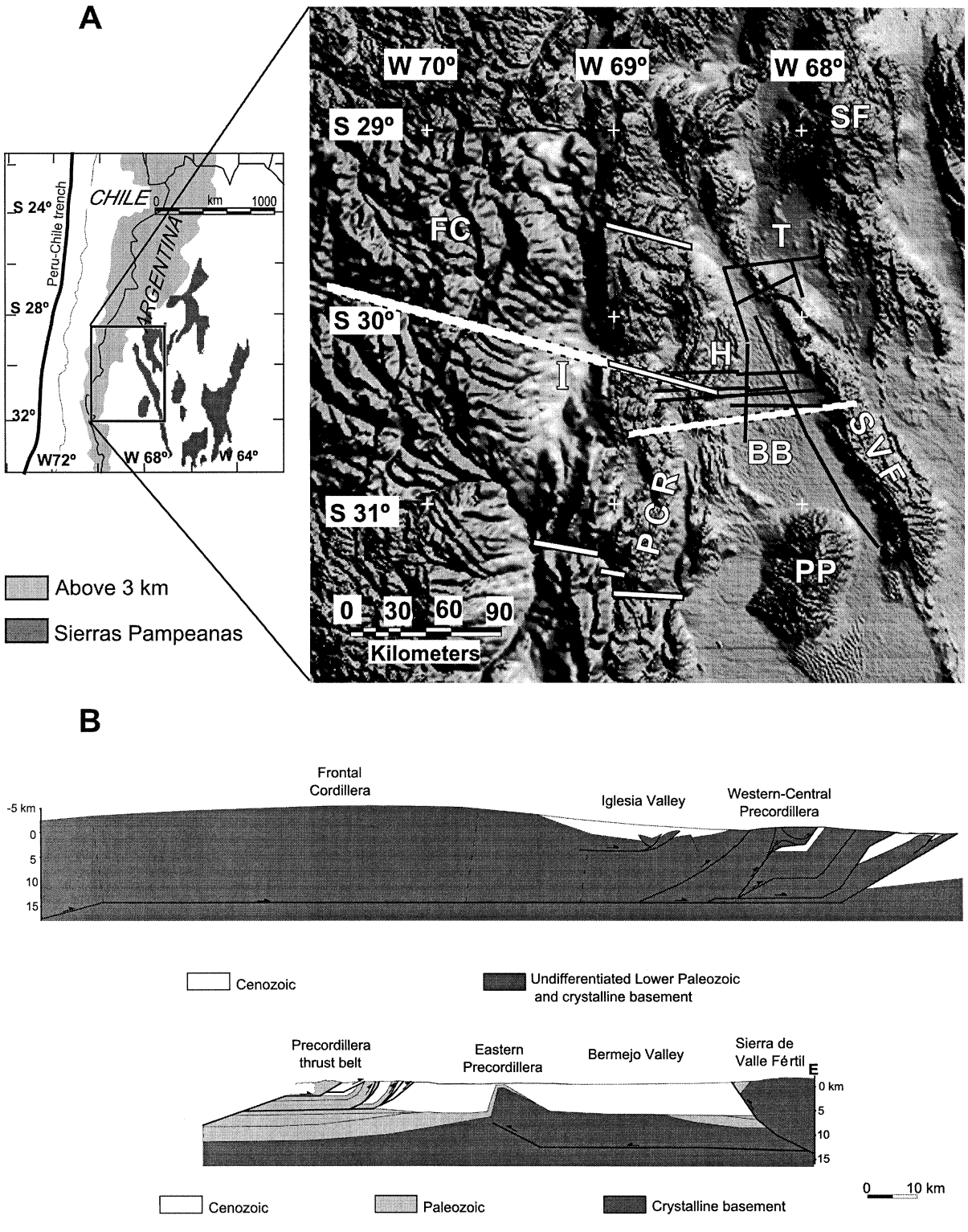

Fig. 1. (A) Shaded Digital Elevation Model of the Bermejo basin system, which encompasses both the modern depositional basins (Bermejo 'BB', Talampaya 'T', and Iglesia 'I' valleys) and the modern mountain ranges (entire zone west of Iglesia Valley is the Frontal Cordillera 'FC', Precordillera 'PCR', and Sierras Pampeanas blocks: Pie de Palo 'PP', Sierra de Valle Fértil 'SVF', Sierra de Famatina 'SF'). White bars with dashed borders show locations of cross-sections below. White bars with solid rims show locations of Fig. 4 cross-sections. Bold black lines are seismic lines (chosen from a much larger grid of seismic data) from which thickness data (Fig. 2) were extracted. (B) Cross-sections through (upper) the Precordillera, Iglesia Valley and Frontal Cordillera (from Allmendinger *et al.*, 1990) and (lower) the modern Bermejo Valley and adjacent ranges (from Zapata & Allmendinger, 1996b).

a well-constrained maximum of about 15 km at 30°15′S (Fig. 4B), to less constrained minima of about 6 km at 31°30′S (Fig. 4A) and 29°30′S (Fig. 4C). The integrated shortening and decollement depth results in crustal thickening estimates of about 10 km at 30°15′S, and 5–6 km at 29°30′ and 31°30′S.

The 20–9 Ma shortening in the east-vergent Precordillera thrust belt is considered to have been

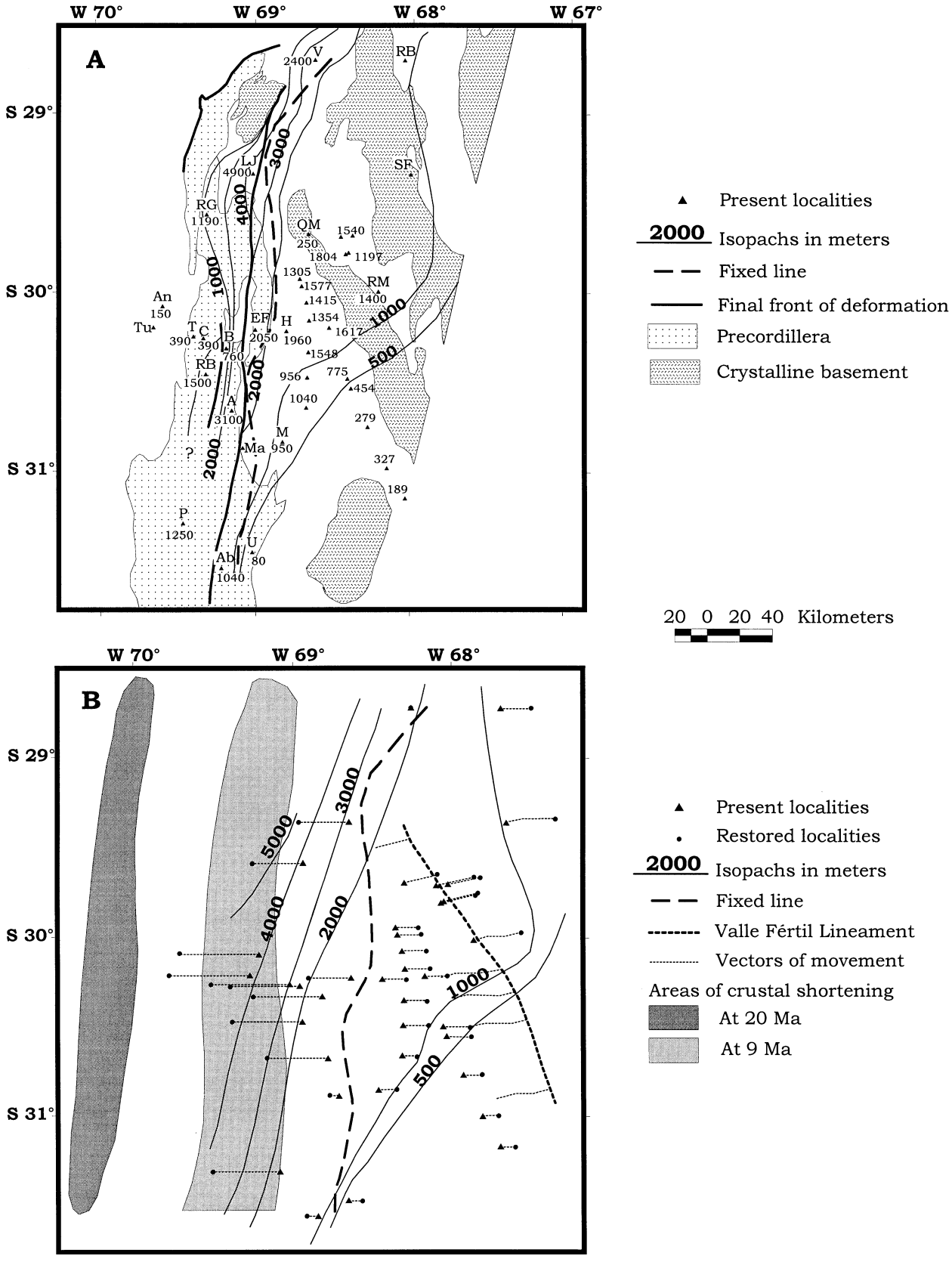

uniform and contemporaneous along strike (Fig. 5). Estimates of the age and amount of shortening at 30°S (Jordan *et al*., 1993a; Zapata & Allmendinger, 1996a,b; Jordan *et al*., 2001) and age constraints for synorogenic sediments at 29°S (Reynolds *et al*., 1990) and 31°S (Bercowski & Figueroa, 1989; Milana, 1991; Milana *et al*., 1993; Bercowski *et al*., 1994) justify this hypothesis. Thrusting began at approximately 20 Ma in the Western Precordillera, followed by a several million year interval of quiescence (Fig. 5). The deformation resumed roughly at 15 Ma, with an interval of most rapid shortening of the Central Precordillera spanning about 12–10 Ma, followed by declining rates (Fig. 5). At about 7 Ma, shortening in the Central Precordillera may have stopped or been very slow (Fig. 5). Note, however, that the constraints on thrust history could be fit by a constant rate of shortening throughout the interval 20 Ma to the present, although we do not favour that interpretation (Fig. 5).

The Calingasta–Iglesia basin separates the Precordillera from the Frontal Cordillera (Fig. 1A,B). Shortening in the Frontal Cordillera between 30° and 31°S is about 8% (Rodríguez Fernández *et al*., 1996), and at 32°S is about 10% (Cristallini & Ramos, 2000). That Frontal Cordillera shortening is much less than Precordilleran shortening suggests that most of the overall Andean crustal shortening is transferred to the Precordillera (Rodriguez Fernández *et al*., 1996). Allmendinger *et al*. (1990) postulated that the Frontal Cordillera between 29° and 31°S is uplifted as a ramp-anticline over a mid-crustal decollement (Fig. 1B). From the mid-crustal detachment geometry (Fig. 1B) and the magnitude of crustal shortening in the Precordillera, Allmendinger *et al*. (1990) estimated 5 km of structural thickening of the crust in the Frontal Cordillera. In the absence of additional data, we generalize this estimate to apply to the Frontal Cordillera to the north and south as well.

The timing of uplift in the Frontal Cordillera between 29° and 31°S is identical to the timing of thrusting in the east-vergent Precordillera thrust belt, if the same decollement controls both ranges (Fig. 1A, Allmendinger *et al*., 1990). For the segment to the north, the time of shortening could differ and is not constrained. South of 31°S nearly all of the upper crustal shortening and thickening (along emergent faults) of the Principal and Frontal Cordillera were completed before 9 Ma (Cristallini & Ramos, 2000).

CRUSTAL LOADS ADDED BETWEEN 20 AND 9 Ma

Load profiles

Spatially and temporally variable crustal shortening created the loads that generated flexural subsidence in the Bermejo foreland basin, but equally variable surface processes eroding and redistributing sediments, distorted the geometry of the tectonically originated loads. The 20–9 Ma loading involved crustal thickening due to tectonic shortening, crustal thinning due to erosion of highlands, and crustal thickening due to accumulation of sediments (Jordan *et al*., 2001). The 9 Ma product of these transient processes in two dimensions was the mountain belt–Bermejo basin cross-sectional configuration shown in Fig. 6(A). The cumulative 20–9 Ma crustal loads (Fig. 6B) are equivalent to the difference in cross-sectional area between the configuration restored to its 9 Ma state (Fig. 6A), and the cross-section restored to its pre-20 Ma state.

A minimum estimate of crustal thickening due to sediment accumulation was obtained by measuring the decompacted cross-sectional area of the 20–9 Ma preserved strata (light grey areas, Fig. 6B). Decompaction is necessary to assess the thickness and density of the sediments at 9 Ma. The effects of 9 Ma decompaction on our sediment accumulation estimates are not the same throughout the Bermejo basin. Near 29°S at Las Juntas (LJ, Figs 2 and 6B), the entire sedimentary section that is preserved today was already deposited at 9 Ma (Fig. 7A).

Fig. 2. Isopach maps of the Bermejo foreland basin for the 20–9 Ma time interval, based on (A) current, and (B) palinspastically restored geographical positions. Data compiled from well-dated surface sections (locations marked by letters) and from industry seismic data tied to the dated outcrops of the Eastern Precordillera (Fernández, 1996; Zapata, 1996). Time line is locally 9.1 Ma on magnetic polarity time sections, but correlation at the basin scale does not justify retaining the decimal point. Preserved compacted thickness given in metres. Restored offsets on faults at 9 Ma are based on the Precordillera shortening history of Fig. 5, and the history of deformation of Zapata & Allmendinger (1996a) and Jordan *et al*. (2001) for the Sierras Pampeanas. On (B) the lengths of the vectors connecting the current geographical positions (triangles) to the restored positions (circles) indicate the cumulative offset of individual points between 9 Ma and today. The latitude/longitude grid and the 'fixed line' separating areas of east- and west-vergent deformation are a fixed framework, against which restored position can be compared. Names of surface sections and sources of data for each are: An = Angualasto, Tu = Tudcum (Jordan *et al*., 1997); T = Quebrada de las Trancas, C = Quebrada Caracol, Rb = Río Blanco, B = Los Blanquitos (Jordan *et al*., 1993a,b), EF = El Fiscal (Jordan *et al*., 1993b; Milana, 1993); RG = Río Gualcamayo (Parker, 1974), LJ = Las Juntas (Reynolds *et al*., 1990), H = Huaco (Johnsson *et al*., 1984, 1986; Beer & Jordan, 1989; Fernández & Jordan, 1996); A = Río Azul (Jordan *et al*., 1990; Milana, 1993), Ma = Matagusanos anticline (Zapata, 1996; Brooks, 1999), M = Sierra de Mogna near Río Colorado (Milana, 1991); QM = Quebrada del Médano (Malizzia & Limeres, 1984; Malizia *et al*., 1995); RM = Río Mañero (Malizia *et al*., 1995), V = Vinchina (Ramos, 1970; V. Ramos, personal communication 1984; Re & Vilas, 1990; Re, 1998), RB = Río Blanco, SF = Santa Florentina (Tabbutt *et al*., 1989); P = Pachaco (Milana *et al*., 1993); Ab = Albaracín (Bercowski & Figueroa, 1989); U = Ullum (Bercowski *et al*., 1986, 1987). An and T are located in the Iglesia basin.

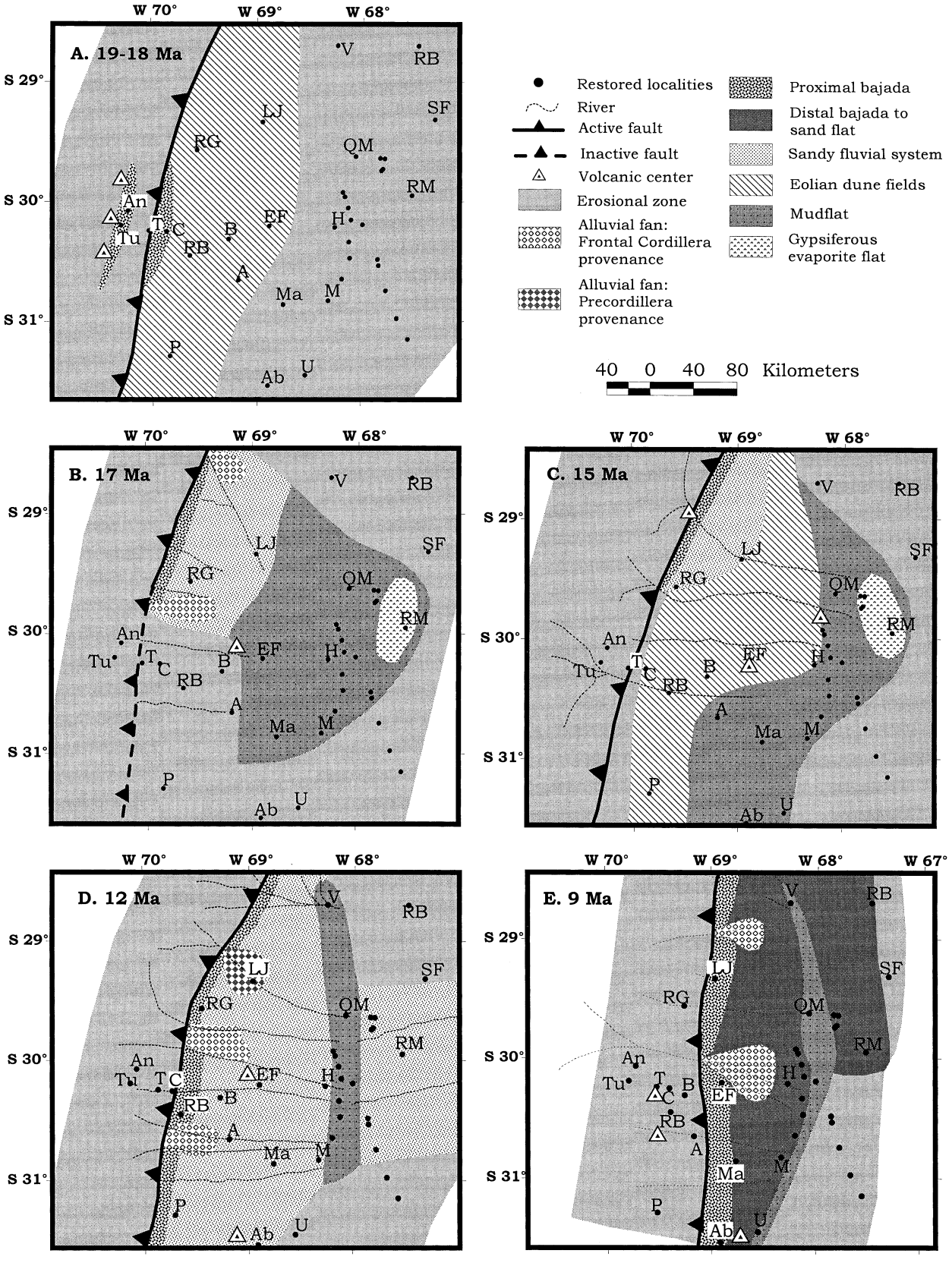

Fig. 3. Depositional environments and palaeogeography at five times in the 'simple foreland' evolution of the Bermejo basin, on palinspastically restored bases. Data for environments and deformation come from Beer & Jordan (1989), Bercowski *et al.* (1986, 1987), Bercowski & Figueroa (1989), Coughlin *et al.* (1998), Damanti (1989), Fernández (1996), Fernández & Jordan (1996), Jordan *et al.* (1990, 1993a,b, 1997), Johnson *et al.* (1986, 1984), Malizia *et al.* (1995), Milana (1991, 1993), Milana *et al.* (1993), Ramos (1970), Re (1995), Reynolds *et al.* (1990), Tabbutt *et al.* (1989), Zapata & Allmendinger (1996a,b), Zapata (1996, 1998). Localities and labelling scheme as in Fig. 2.

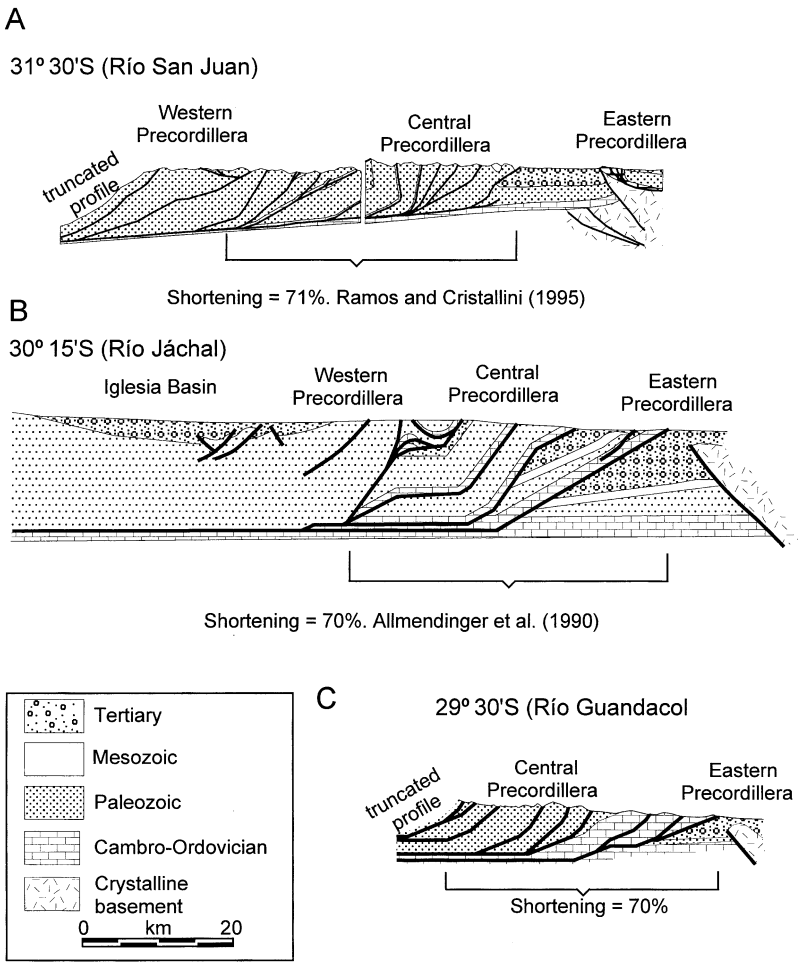

Fig. 4. Structural cross-sections of the Precordillera thrust belt at three latitudes. Section C is derived from published (Furque, 1963; Baraldo, 1985; Astini, 1991; Zambrano *et al.*, 1996) and new field data collected by N. Cardozo. See Fig. 1 for locations.

Assuming that a significant thickness of younger strata were not erosionally lost, there would have been no incremental compaction since 9 Ma. In contrast, burial of the 20–9 Ma strata at Huaco (H, Figs 2, 6B) by ~3500 m of younger strata would have provoked compaction by ~400 m (Fig. 7A, Damanti & Jordan, 1989). Correcting the stratal thickness to the 9 Ma state adds 15% to the total thickness of 20–9 Ma preserved strata at Huaco but nothing at Las Juntas (Fig. 7A). We performed one-dimensional decompaction (Sclater & Christie, 1980) of the 20–9 Ma strata at model localities more than 20 km away from Las Juntas. In the absence of additional data, we assumed that the compaction behaviour of the Bermejo and Iglesia–Calingasta strata was similar throughout the basin, and was characterized by porosity–depth relations empirically derived at Huaco (Damanti & Jordan, 1989, their Appendix 1). The errors in the 20–9 Ma sedimentary thickness estimation introduced by this assumption do not exceed 10% of the estimated total columnar thickness at any location.

Estimates of 20–9 Ma crustal thinning due to erosion of highlands are the least constrained. A long-term west to east sediment transport vector derived from palaeocurrent data (Beer & Jordan, 1989; Milana, 1990a,b) and clast compositions of the Bermejo strata (Damanti, 1989; Jordan *et al.*, 1990; Reynolds *et al.*, 1990; Jordan *et al.*, 1993a,b) confirm that the Frontal Cordillera and Precordillera were the source areas of virtually all exposed clastic detritus in the Bermejo basin (Jordan *et al.*, 2001). In theory, the proportion of Frontal Cordillera vs. Precordillera transferred mass can be quantified by measuring in the Bermejo basin sediments the ratio of Precordillera sedimentary lithic grains (Ls) to Frontal Cordillera volcanic lithic grains (Lv) (Damanti, 1989; Jordan *et al.*, 1990; Reynolds *et al.*, 1990; Jordan *et al.*, 1993a). But mechanical weathering preferentially enhances Lv and makes the Lv/Ls ratio unreliable to quantify provenance (Jordan *et al.*, 2001). Even though a proportion of the sediments derived from each source area cannot be established, the available data suggest that the relative importance of the Frontal Cordillera and Precordillera as source areas varied through time and space (Jordan *et al.*, 2001).

In our model, 20–9 Ma crustal thinning due to erosion of the Precordillera highlands was estimated by assuming that erosion lowered the upper envelope of the structural cross-section (Fig. 6A) to a long-wavelength, critical slope. For the Río San Juan and Río Guandacol, we imposed a 2° upper slope to the 9 Ma structural profile (Fig. 6A), similar to the regional slope exhibited today

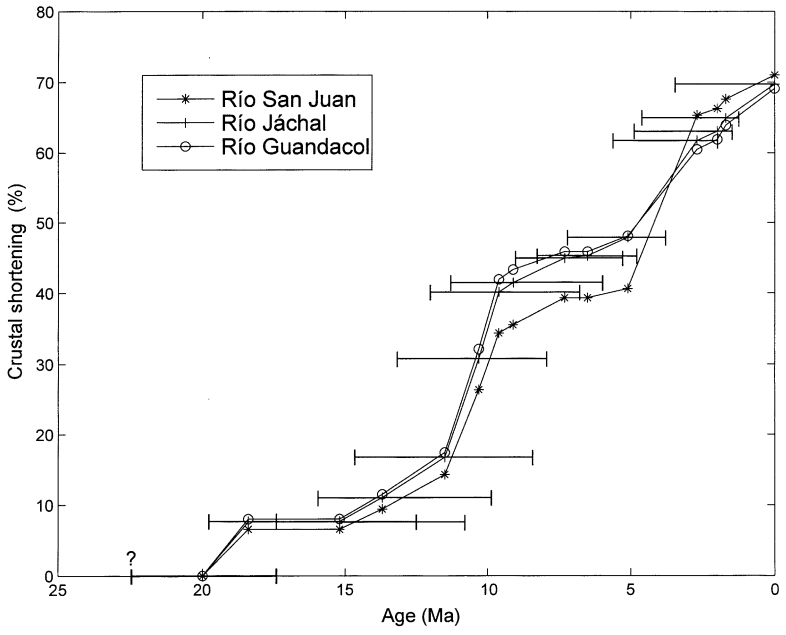

Fig. 5. Crustal shortening history of the Precordillera at Río San Juan, Río Jáchal and Río Guandacol. Although error bars are not shown on shortening, the estimated shortening is based on the assumption of minimum erosional gaps between restored thrust plates and therefore it represents a minimum estimate of horizontal deformation for the choice of decollement depth. Timing of deformation is based on Jordan *et al.* (1993a) and Zapata & Allmendinger (1996a,b) for the Río Jáchal, Milana *et al.* (1993) and Bercowski *et al.* (1994) for the Río San Juan and Reynolds *et al.* (1990) for the Río Guandacol. The graph is constructed on the assumption that the shortening on each thrust accumulated steadily over the time span in which it was active. Time error bars in the Río Jachal crustal shortening history illustrate uncertainty between our preferred interpretation and the maximum deformation span supported by data. Time error bars for the Río San Juan and Río Guandacol curves are likely larger, due to less complete documentation.

across the Andean thrust belt at 32°S (Cristallini & Ramos, 2000). In the Río Jáchal 9 Ma cross-section, a surface slope was linearly interpolated from the Western Precordillera (with a minimum crustal thickening of 10 km, Allmendinger *et al.*, 1990) to the proximal El Fiscal columnar section (EF, Figs 2 and 6A). The resultant Precordilleran eroded sediments (areas between dashed lines and surface slopes in Fig. 6A) are 45% of the 20–9 Ma Bermejo sedimentary areas in the Río San Juan and Río Jáchal profiles, and 30% in the Río Guandacol profile. Implicitly, the remaining sedimentary volume must have come from the Frontal Cordillera. Our results are quite insensitive to the accuracy of the above erosional unloading estimates. 20–9 Ma erosional unloading in the Frontal Cordillera does not produce any flexural response in the Bermejo basin (as we show later), and in the Precordillera at the Río Jáchal latitude it is just 10% of the crustal thickening (Fig. 6A).

The integrated product of 20–9 Ma Frontal Cordillera and Precordillera deformation, erosion of highlands, and redistribution of the sediments is illustrated in two dimensions by the discretized load profiles of Fig. 6(B) ($\times 2$ vertical exaggeration). Additionally, interpolation of the load profiles along strike allowed the construction of three-dimensional load surfaces (Fig. 11A). The load profiles (or surfaces) represent the crustal thickness added during 20–9 Ma. The Frontal Cordillera and Iglesia–Calingasta basin load configurations are similar along strike (Fig. 6B). The Precordillera exhibits crustal thickening maxima that vary along strike, from about 9 km at the Río Jáchal to about 5 km at the Río San Juan and Río Guandacol (Fig. 6B). The Bermejo basin displays a crustal thickening that increases to the north (Figs 2 and 6B).

In order to quantify the stress imposed on the lithosphere by the 20–9 Ma accumulated loads, one needs to know the average density of the rock column at every location. For the thrust belt material (dark grey areas, Fig. 6B) we assumed an average density (ρ_t) of 2700 kg m^{-3}, a reasonable estimate for well-compacted, siliciclastic, thrust sheet rocks (Turcotte & Schubert, 1982; Stockmal & Beaumont, 1987). For the Bermejo and Iglesia–Calingasta sediments (light grey areas, Fig. 6B), we estimated the average columnar density based on the burial history of the sediments at Las Juntas and Huaco (Fig. 7A), and empirically derived porosity–depth relations at these localities (Reynolds *et al.*, 1990; Damanti & Jordan, 1989). Assuming an average grain density of 2650 kg m^{-3} and full water saturation of the sediments, we computed the change of average columnar density with total columnar thickness (Fig. 7B). By extrapolating the average density–total thickness relation at Las Juntas to localities closer than 20 km from it, and the Huaco relation to all other localities, we constructed a 9-Ma sedimentary density field (ρ_s). The computed density

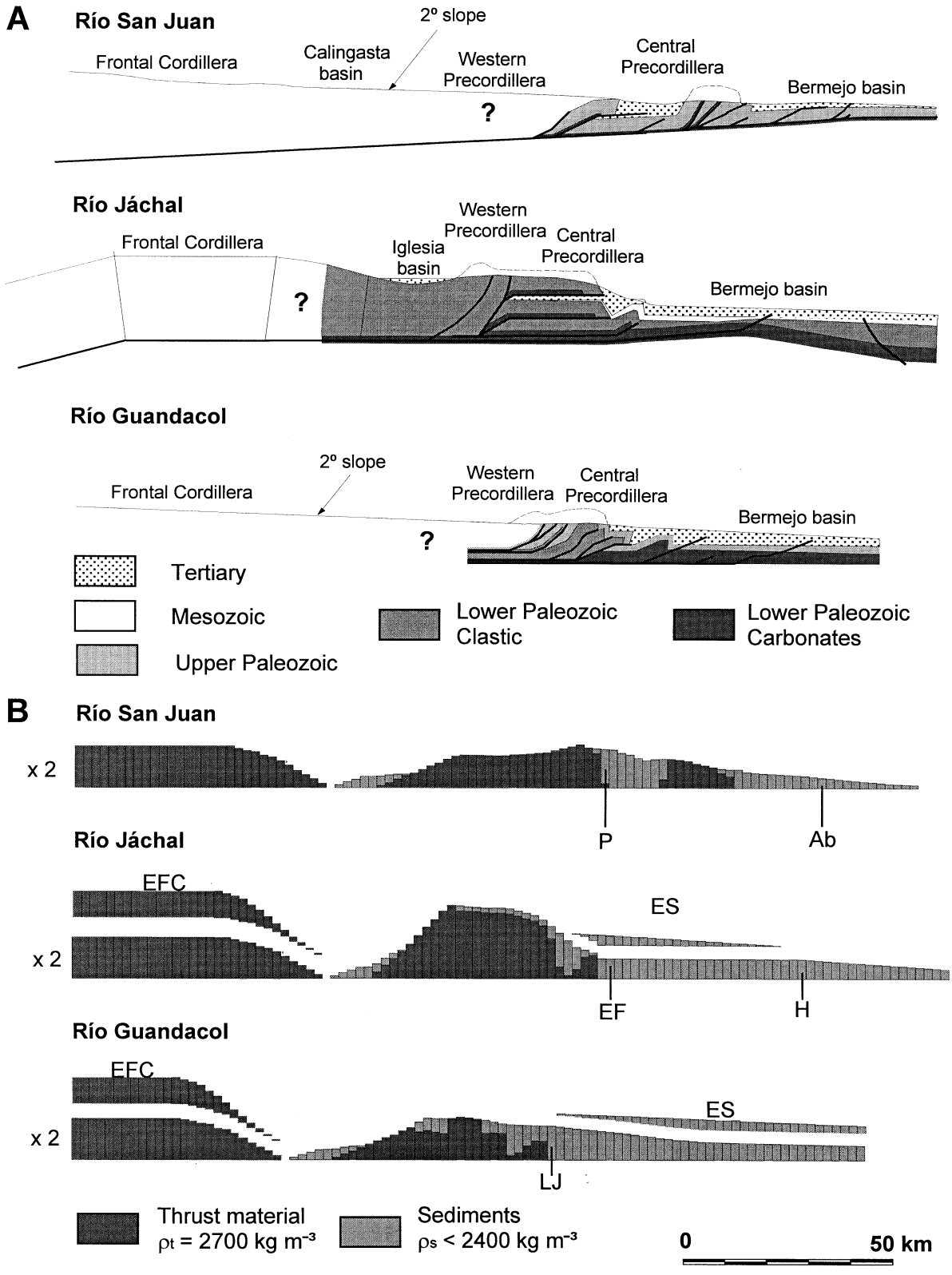

Fig. 6. (A) Palinspastic 9 Ma mountain belt–Bermejo basin cross-sectional configurations at three latitudes. These differ from Fig. 4 by restoration of folds and faults that are younger than 9 Ma. The area between the dashed line and the 9 Ma surface represents the sediments eroded from the Precordillera highlands during the 20–9 Ma interval. (B) 20–9 Ma crustal thickening areas (× 2 vertical exaggeration). These are crustal loads when multiplied by density and gravity. The small areas above the 20–9 Ma load profiles labelled ES (enhanced proximal sedimentation) and EFC (enhanced Frontal Cordillera loading) show additional loads which, summed with the rest of the load, provide alternative load configurations tested in our mechanical models. Initials below the 20–9 Ma load profiles are along-strike projections of selected Bermejo basin columnar sections (Fig. 2).

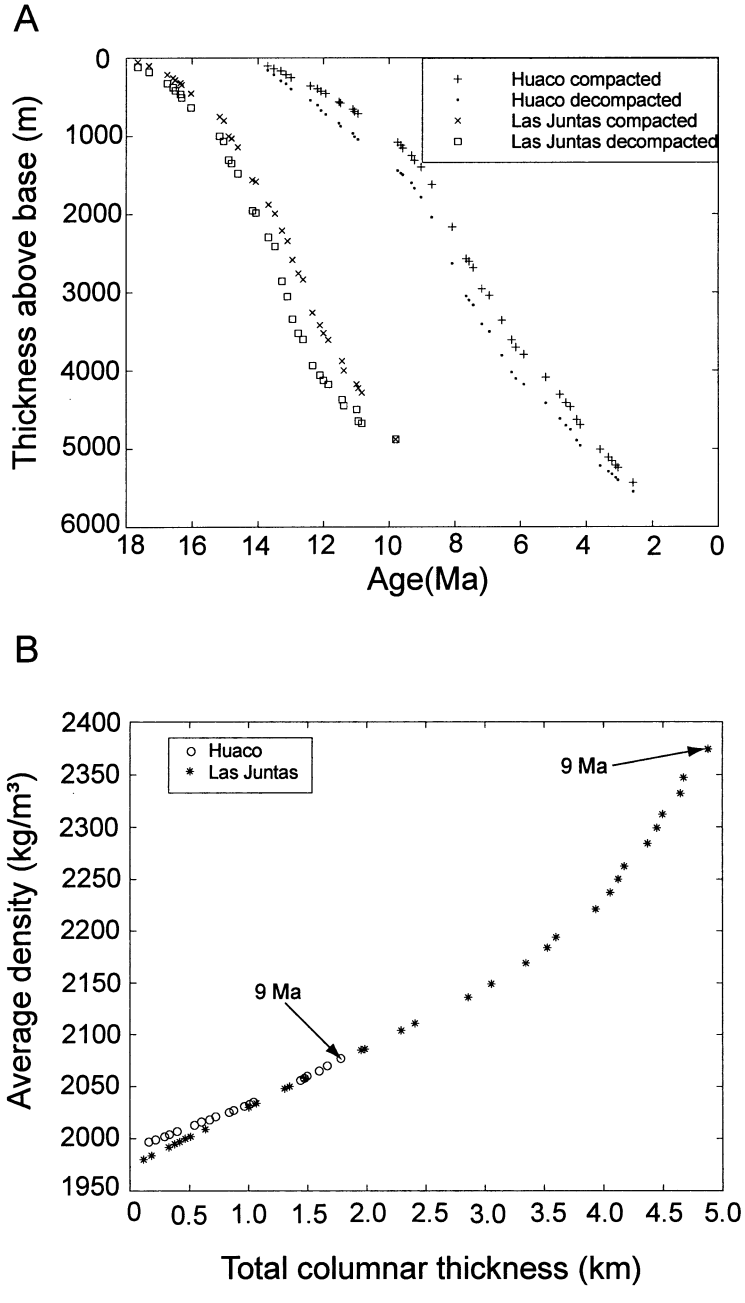

Fig. 7. (A) Sediment accumulation history, and (B) change of average columnar density with total thickness at Huaco and Las Juntas. The sediment accumulation history graph compares the present thicknesses of dated intervals to the thickness that would have existed during progressive burial. Arrows in (B) indicate the 9 Ma average density at these localities. The graphs are based on empirical equations derived by Damanti & Jordan (1989, their appendix 1) for Huaco and Reynolds *et al.* (1990, their appendix A) for Las Juntas. Changes of average density with total thickness are computed assuming a granular density of 2650 kg m^{-3} and full water saturation of the sediments.

field (ρ_s) increases northward in the proximal Bermejo basin, from values of 2050–2100 kg m^{-3} near 30°S (EF, H, Figs 2 and 7B), to a maximum value of 2380 kg m^{-3} near 29°S (LJ, Figs 2 and 7B).

These loads are the input to the mechanical models. The validity of the mechanical model is judged by the similarity of the model's generated topography to the facies patterns. Therefore, we avoid circular reasoning by using only data that constrain crustal thickening and thinning as input, but not facies data as input.

MECHANICAL MODELS

The 20–9 Ma mountain belt to Bermejo basin system developed on a lithosphere that overlay a normally subducting (30°) slab (Kay *et al.*, 1988). The mechanical processes that shaped the loads in the system were transient, but probably the mechanical link between the mountain belt and the foreland basin at any instant was static (time independent, Jordan, 1981, 1995). As an initial simple model, we hypothesize that flexural deformation of an elastic lithosphere beside a thickened mountain belt explains the 20–9 Ma tectonic subsidence pattern observed in the Bermejo basin. Failure of this static (time independent) mechanical model to fit observations would nullify our hypothesis.

Three mechanical models were explored in our analysis: 2D flexure of an infinite, constant thickness elastic lithosphere; 3D flexure of an infinite, constant thickness elastic lithosphere; and 3D flexure of an infinite,

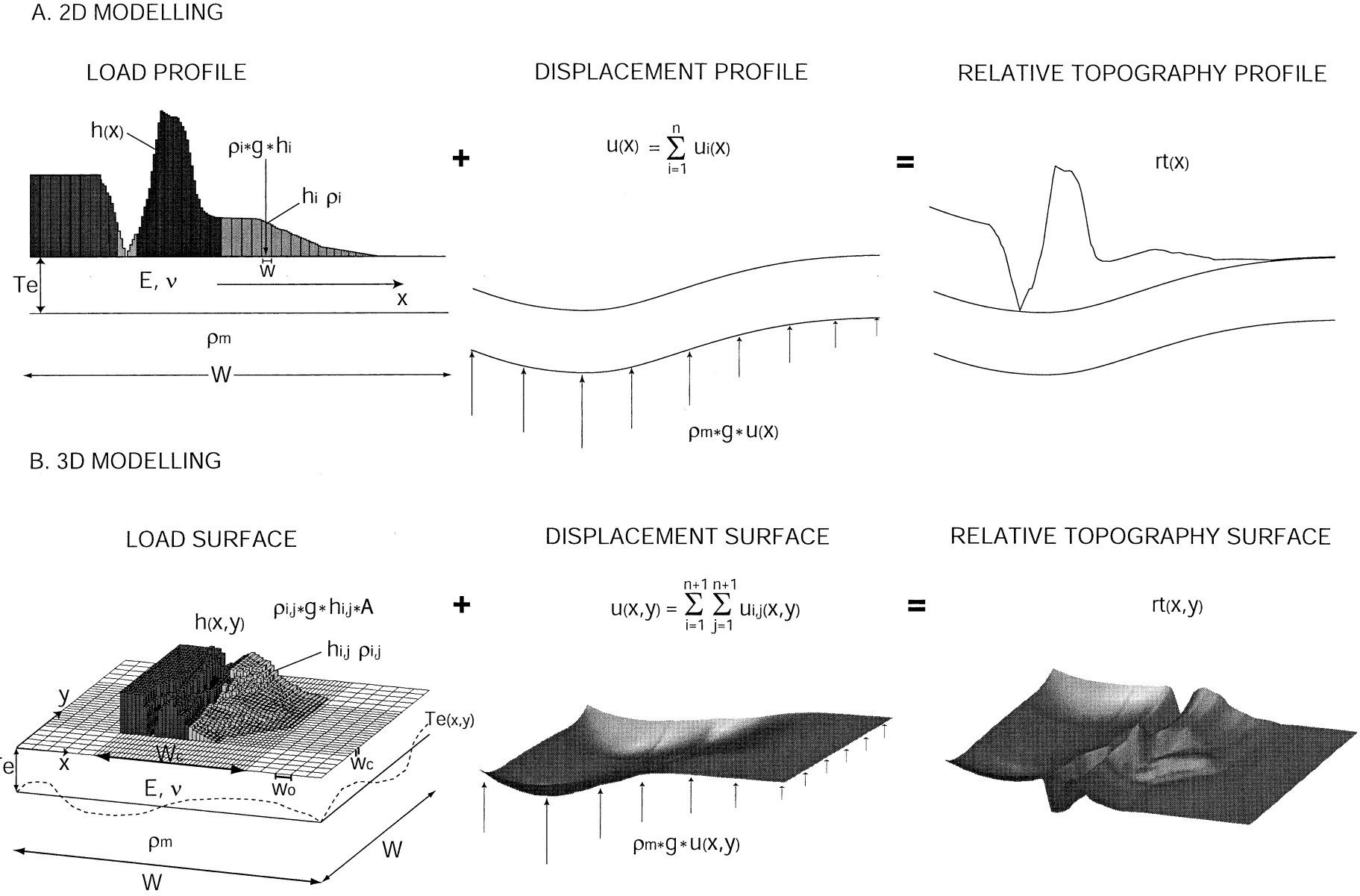

Fig. 8. Conceptual description of our mechanical models. (A) 2D and (B) 3D loading of an elastic lithosphere overlying a semifluid asthenosphere. (A) is solved analytically using the analogy of an infinite beam on an elastic foundation (Hetényi, 1946). (B) is solved analytically using the analogy of an infinite plate on an elastic foundation (Timoshenko & Woinowsky-Krieger, 1959), and numerically using the finite element method (Zienkiewicz, 1977). The model output is a relative topography profile or surface (*rt*) that results from the sum of a known imposed load profile or surface (*h*) and a displacement profile or surface (*u*). In load profile and surface, dark and light grey denote thrust and sedimentary material, respectively. Constants and variables explained in the text.

variable thickness elastic lithosphere. Our strategy is to test whether the mechanical assumptions successfully explain the geometry of the 9 Ma Bermejo basin. The 2D elastic model serves as an initial template for this purpose. If the results do not fit the observed geometry of the basin, the mechanical assumptions are invalidated.

Two-dimensional flexure of an elastic lithosphere overlying a semifluid asthenosphere, ignoring horizontally applied forces, is described by the differential equation (Hetényi, 1946; Turcotte & Schubert, 1982)

$$D\frac{\mathrm{d}^4u}{\mathrm{d}x^4} = \rho(x)gh(x) - \rho_m g u(x) \quad (1)$$

where D is the flexural rigidity ($ET_e^3/12[1-\nu^2]$), x is a coordinate axis, $u(x)$ is the vertical displacement, $\rho(x)$ is the density of the load material, g is the Earth's gravitational acceleration, $h(x)$ is the height of the load, ρ_m is the density of the mantle, E is Young's modulus, ν is Poisson's ratio, and T_e is the elastic thickness. Note that the restoring force (second term in right side of eqn 1) is proportional to ρ_m, since we are interested in the deformation produced by a 'known' 9 Ma load configuration (Turcotte & Schubert, 1982). Table 1 shows the values adopted for these mechanical parameters.

For an infinite, constant elastic thickness lithosphere under constant distributed loading, the analytical solution of eqn 1 provides a small set of equations (Hetényi, 1946, his equations 7, 8, and 9). Our 2D modelling strategy involved the discretization of the area below the load profile (of variable height $h(x)$ and width $W = 350$ km) into ($n = 175$) small rectangles of equal width ($w = 2$ km), but different height (h_i) and density (ρ_i) (Table 1, Fig. 8A). The deflection profile ($u_i(x)$) produced by the load of each one of these elements ($\rho_i * g * h_i$) was then computed based on Hetényi (1946) equations. The total displacement profile ($u(x)$, Fig. 8A) is equal to the sum of all the deflection profiles of the rectangular elements. The sum of the load profile ($\rho(x)$) and the displacement profile ($u(x)$) is the relative topography profile ($rt(x)$, Fig. 8A).

Three-dimensional flexure of an elastic lithosphere was estimated analytically using the analogy of a thin lithospheric plate overlying a semifluid asthenosphere (Timoshenko & Woinowsky-Krieger, 1959). The fundamental assumptions of this model are a small deflection of the mid-surface of the lithospheric plate in comparison with its elastic thickness, negligible vertical shear strains, and no mid-surface straining (Ugural & Fenster, 1995). The vertical displacement of the lithosphere is governed by the equation (Timoshenko & Woinowsky-Krieger, 1959)

$$\frac{\partial^4 u(x,y)}{\partial x^4} + 2\frac{\partial^4 u(x,y)}{\partial x^2\,\partial y^2} + \frac{\partial^4 u(x,y)}{\partial y^4} = \frac{\rho(x,y)gh(x,y)}{D} - \frac{\rho_m g u(x,y)}{D} \quad (2)$$

where y is an additional coordinate axis. The analytical solution of eqn 2 for an infinite, constant elastic thickness lithosphere carrying a point load is an equation involving Bessel functions (Timoshenko & Woinowsky-Krieger, 1959, their Eq. 179). Based on this equation, we implemented our 3D analytical modelling. The volume under the load surface ($h(x, y) * W * W = h(x, y) * 800$ km $*$ 800 km) was discretized into ($n * n = 8100$) prisms with base areas of ($A = w_c * w_c = 5$ km $* 5$ km) in a central region of ($A = W_c * W_c = 400 * 400$ km), or ($A = w_o * w_o =$ 40 km $* 40$ km) and ($A = w_c * w_o = 5$ km $* 40$ km) in outer surrounding regions (Table 1, Fig. 8B). The central region encompassed our area of interest, which was far away from the edge of the model domain in order to avoid side-effects. The force contributions of the prisms ($\rho_{i,j} * g * h_{i,j} * A$) were computed and appropriately

Table 1. Model Input Parameters.

Mechanical Parameters

$E = 70.0$ GPa
$\nu = 0.25$
$T_e = 10.0$–50.0 km
$\rho_t = 2700.0$ kg m^{-3}
$\rho_t = 1950$–2400 kg m^{-3}
$\rho_t = 3300$ kg m^{-3}
$g = 9.8$ m s^{-2}

Geometrical Parameters

	Units	2D	3D Analytical	3D Numerical
W	km	350.0	800.0	800.0
W_c	km	–	400.0	400.0
n		175	90	90
w	km	2	–	–
w_c, w_o	km	–	5, 40	5, 40
z_d		1	1	5
N	km	175	8100	40 500

summed at every node location (i, j). The deflection surface produced by each nodal force ($u_{i,j}(x, y)$) was computed based on the Timoshenko & Woinowsky-Krieger (1959) equation, and from the sum of all the nodal deflection surfaces the total displacement surface was calculated ($u(x, y)$, Fig. 8B). The relative topography surface ($rt(x, y)$, Fig. 8B), the output of our 3D model, is equal to the sum of the load surface ($h(x, y)$) and the displacement surface ($u(x, y)$).

Three-dimensional flexure of a continuous, homogenous, isotropic, linear, elastic body was also estimated using the finite element method (Zienkiewicz, 1977; Huebner *et al.*, 1995). The purpose of this strategy was two-fold: to have an independent test of the correctness of our 3D analytical implementation, and to be able to explore the effects of lateral changes in elastic thickness of the lithosphere. For elasticity, the governing differential equations are the equilibrium equations (Ugural & Fenster, 1995)

$$\begin{aligned}
&\frac{\partial \sigma_x}{\partial x} + \frac{\partial \sigma_{xy}}{\partial y} + \frac{\partial \tau_{xz}}{\partial z} + X = 0 \\
&\frac{\partial \tau_{xy}}{\partial x} + \frac{\partial \sigma_y}{\partial y} + \frac{\partial \tau_{yz}}{\partial z} + Y = 0 \\
&\frac{\partial \tau_{xz}}{\partial x} + \frac{\partial \tau_{yz}}{\partial y} + \frac{\partial \sigma_z}{\partial z} + Z = 0
\end{aligned} \tag{3}$$

where x, y and z are coordinate axes, σ are normal stresses, τ are shear stresses, and X, Y, Z are body forces, per unit volume. The finite element formulation of eqn 3 for a discretized system with m nodes is (Huebner *et al.*, 1995)

$$\begin{bmatrix} {}^{3m\times 3m} \\ K \end{bmatrix} \begin{Bmatrix} {}^{3m\times 1} \\ \delta \end{Bmatrix} = \begin{Bmatrix} {}^{3m\times 1} \\ F \end{Bmatrix} \tag{4}$$

where $[K]$ is the system stiffness matrix, $\{\delta\}$ is a column vector of nodal displacement components for the entire system, and $\{F\}$ is the column vector of resultant nodal forces.

Equation 4 was solved using ABAQUS/Standard 5.8^{TM}, a general-purpose finite element program. The finite element discretization followed the geometry introduced in the 3D analytical implementations, with the difference that the spatially variable vertical dimension was discretized in 5 (z_d) rows (Table 1). Thus, the 3D domain was discretized in 40 500 (N) eight-node tetrahedral elements (Table 1).

MODEL RESULTS

Two-dimensional modelling

The simplest experiment to evaluate the effects of 20–9 Ma crustal loads on the tectonic subsidence in the Bermejo basin is to compute in two dimensions the flexural deformation produced by the documented 9 Ma load profiles (Fig. 6B) on an infinite, elastic lithosphere of constant thickness. The modelled 9 Ma topography is equal to the sum of a pre-20 Ma depositional profile, the thickness of the load added, and the profile of lithospheric flexural deformation. Given our lack of constraints on the palaeo-elevation of the pre-20 Ma depositional profile (unconformity), we have assumed an initially flat pre-20 Ma profile in all our simulations. Thus, the resultant topography profiles (black lines in Fig. 9) display the elevation across strike of the 9 Ma mountain belt–foreland basin system relative to a flat pre-20 Ma unconformity. The assumption about palaeo-topography and neglect of along-strike flexure undoubtedly introduce errors. Nevertheless the 9 Ma modelled topography profiles are invaluable to identify trends in palaeo-surface elevations, assess the sensitivity to elastic thickness changes, identify major discrepancies between model results and geological observations, and formulate remedial measures or alternative load configurations.

Three models of 9 Ma topography, for three different elastic thicknesses, produce similar geometries (black lines, Fig. 9), in spite of dissimilar flexural deflection profiles (grey lines, Fig. 9). The configuration of the load (i.e. amplitude and wavelength) dominates over the flexural response. The 9 Ma topography profiles that result from deformation of a 10-, 30- or 50-km elastic lithosphere show a large (3–4 km) depression in the Iglesia–Calingasta basin, a 2–6 km high Precordillera, a Bermejo basin above sea level, and a well-developed forebulge (200–1000 m) in the medial Bermejo basin along the Río Jáchal and Río Guandacol sections (Fig. 9). The field of vertical deformation produced by the 20–9 Ma crustal loads is hardly varied by uniformly weakening or stiffening the underlying elastic lithosphere.

The large Iglesia–Calingasta basin depression is unrealistic. There are no data that suggest that the pre-20 Ma unconformity in the Iglesia–Calingasta Valley was at an altitude more than a few hundred metres above the altitude of the same surface to the east. It is well known that the 20–9 Ma strata of the Iglesia basin accumulated above sea level (Beer *et al.*, 1990; Jordan *et al.*, 1997), yet these models (Fig. 9) imply surface topography at least 2 km below the original datum, and likely below sea level. The obvious discrepancy between the model and the geological observations suggests that the linking mechanism between loading in the Frontal Cordillera and Precordillera and tectonic subsidence in the Iglesia–Calingasta basin was not flexural deformation of an infinite elastic lithosphere. Perhaps local isostatic compensation prevailed in the Frontal Cordillera, and the axis of the Iglesia–Calingasta basin coincided with the broken end of a finite elastic lithosphere (Stewart & Watts, 1997). We did not implement this situation in our mechanical models for two reasons: for the sake of simplicity in our simulations, and to evaluate the maximum possible effects of Frontal Cordillera loading on tectonic subsidence in the Bermejo Basin.

The 2D topography profiles are also inconsistent with the palaeotopography of the 9 Ma Bermejo basin. The 9 Ma depositional environment configuration (Fig. 3E)

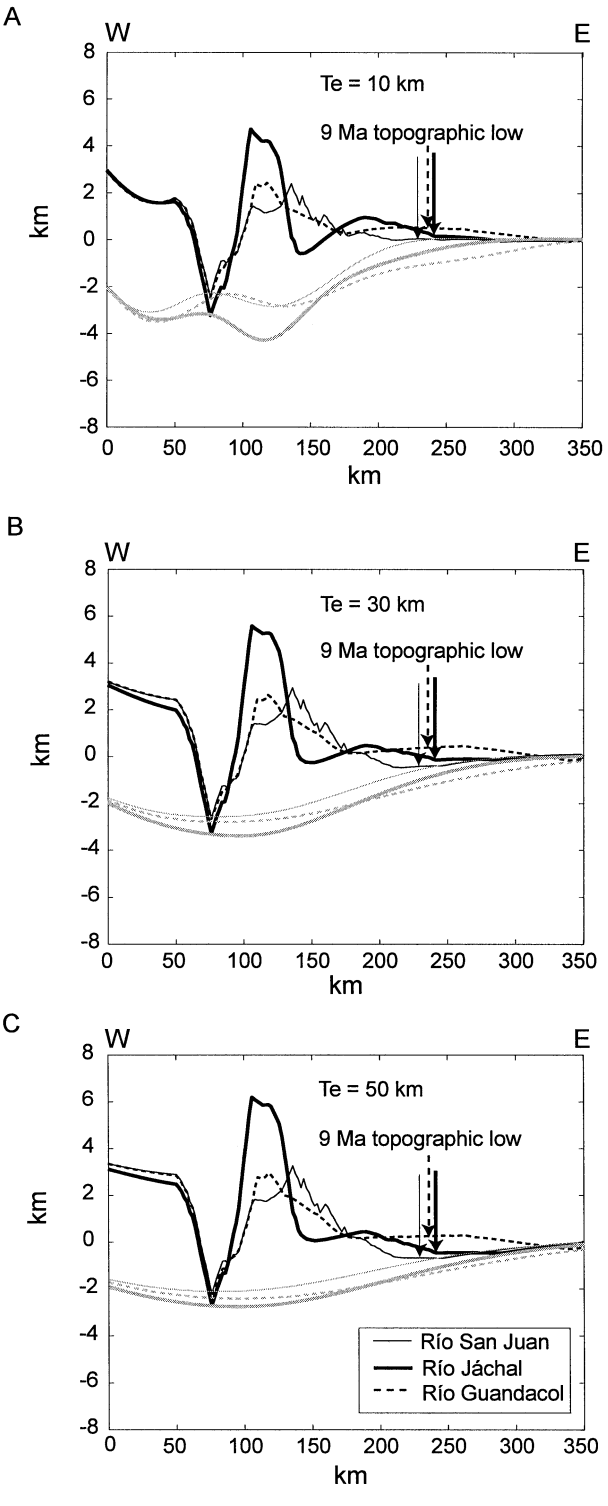

Fig. 9. 9 Ma relative topography profiles (black lines) and flexural deflection profiles (grey lines) at Río San Juan, Río Jáchal and Río Guandacol for a constant elastic ($E = 70$ GPa, $\nu = 0.25$) thickness lithosphere of (A) 10, (B) 30, and (C) 50 km. The profiles display topography relative to an assumed sea level pre-20 Ma unconformity. The arrows (one for each latitude) indicate the approximate palinspastic location of the Bermejo basin axis or topographic low at 9 Ma from Fig. 3(E). Note the similarity of the relative topography profiles for the three elastic thickness cases.

shows drainage systems flowing eastward from the Precordillera towards a muddy basin axis or topographic low; and westward from source areas east of the topographic low (RM, Fig. 3E). The documented 9 Ma topographic low (vertical arrows, Fig. 9) fits reasonably well in the modelled topography at the Río San Juan section, but in the Río Jáchal and Río Guandacol it is actually east of or on the modelled forebulge. The drainage that would form on the modelled topography would flow opposite to the documented drainage, from a source in the medial Bermejo basin (e.g. forebulge) westward towards a localized depression, and eastward towards a distal relatively flat basin (Fig. 9).

Effect of enhanced proximal sedimentation and frontal cordillera loading

The discrepancy between the modelled topography and documented palaeo-drainage has the spatial attributes of a situation of a high rate of accommodation compared to sediment supply: a localized proximal depression and a well-developed medial forebulge. The modelled tectonic subsidence exceeds unrealistically the sediment supply in the proximal Bermejo basin, and the modelled basin's width is smaller than the width of the 9 Ma basin (Fig. 9).

Two remedial measures may improve the ratio of subsidence to sediment supply in the proximal foreland basin: enhanced proximal sedimentation, and enhanced Frontal Cordillera loading. The first correction acknowledges post-9 Ma erosion of the 20–9 Ma strata. Near 30°S at Huaco (H, Figs 2 and 6B) the 20–9 Ma sedimentary section is complete (Beer, 1990), but in the western flank of the basin at El Fiscal (EF, Figs 2 and 6B) the section is incomplete (i.e. its top has been erosionally removed). The loads used in the first experiment (Fig. 9) are correct for the 20–9 Ma strata at Huaco, but ignore the thickness of the 20–9 Ma strata eroded from El Fiscal. To compensate, a revised load profile across the proximal basin that might have existed at 9 Ma was generated by interpolating a gentle slope (2°) from the medial Bermejo basin to the Central Precordillera; the height between the 2° slope and the preserved strata is the eroded strata (labelled ES in Fig. 6B). Note that this 2° slope into the medial foreland basin is *not* the topography; the topography would be derived by subsidence of that slope. The maximum thickness of eroded strata is estimated to be 1250 m. The 9 Ma 'enhanced proximal sedimentation' load profiles are the sum of the initially prescribed 9 Ma load configurations (Fig. 6B) and the estimated cross-sectional areas of eroded strata (ES, Fig. 6B). The second correction might reduce the tectonic subsidence in the proximal Bermejo basin, by enhancing a forebulge induced by the Frontal Cordillera. The correction for enhanced Frontal Cordillera loading acknowledges our lack of constraints on the internal geometry and chronology of deformation of the Frontal Cordillera. The modified 9 Ma load profiles were constructed by

adding 3 km of crustal thickening in the Frontal Cordillera (areas labelled EFC in Fig. 6B) to the initially prescribed 9 Ma load profiles (Fig. 6B).

Figure 10 shows the Río Jáchal topography profiles produced by these 9 Ma modified load configurations, on elastic lithospheres of 10, 30 and 50 km. The effect of enhanced proximal sedimentation is two-fold: it provides enough sediment to fill the proximal depression, and it increases the wavelength of the deformation, moving the forebulge to the east (Fig. 10, e.g. Jordan, 1981; Schlunegger *et al.*, 1997). The addition of some non-preserved 20–9 Ma sediments in the proximal Bermejo basin is mandatory if any flexural model is to replicate successfully the 9 Ma basin's palaeotopography (Fig. 3E). Enhanced Frontal Cordillera loading has minimum effect on the tectonic subsidence in the Bermejo basin. In a weak lithosphere ($T_e = 10$ km), the location of the forebulge induced by an additional 3 km of Frontal Cordillera thickening is at the most proximal Bermejo section, but the additional uplift barely exceeds 50 m (Fig. 10A). In a stronger lithosphere ($T_e = 50$ km) the forebulge induced by the Frontal Cordillera is east of the most proximal Bermejo basin section, in which there is tectonic subsidence that exacerbates the misfit of model to geology (Fig. 10C). This demonstrates that, even if the lithosphere were uniformly strong from the Frontal Cordillera to the Bermejo basin, the Frontal Cordillera load is a weak control at the distance of the proximal Bermejo basin. Given that the Calingasta–Iglesia basin topography surface is completely inconsistent with the hypothesis that there is a strong plate across the western part of our model domain, the Frontal Cordillera is here shown to be of no importance in the mechanical system of the Bermejo basin, except as a source of sedimentary load.

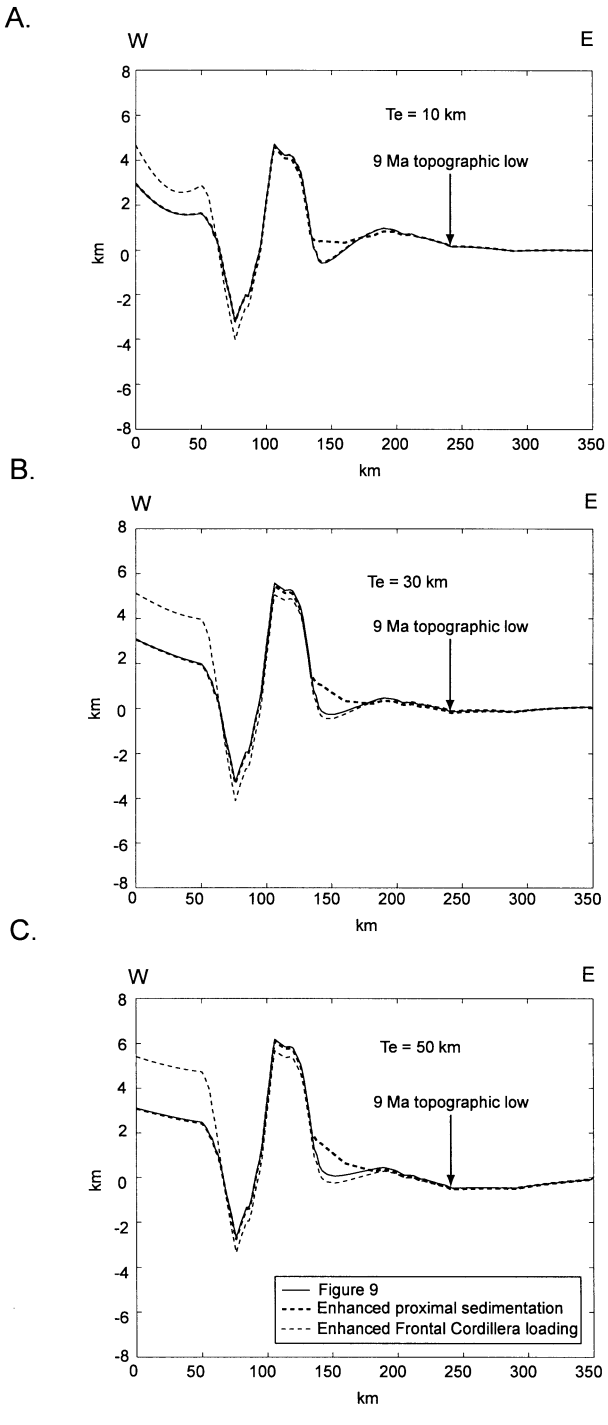

Fig. 10. Effects of enhanced proximal sedimentation and Frontal Cordillera loading on 9 Ma relative topography profiles at Río Jáchal for a constant elastic ($E = 70$ GPa, $\nu = 0.25$) thickness lithosphere of (A) 10, (B) 30 and (C) 50 km. Enhanced Bermejo basin or Frontal Cordillera load profiles are constructed by adding to the load profiles of Fig. 6(B) the EPS and EFCL areas above them.

Three-dimensional modelling

The 3D effects of 20–9 Ma crustal loads on tectonic subsidence in the Bermejo basin are next computed for a lithosphere of constant elastic thickness. Two 9 Ma load configurations were tested: a load surface resulting from interpolation of the preserved load profiles of Fig. 6(B) (left side, Fig. 11A), and an enhanced proximal sedimentation load surface (left side, Fig. 11B). The difference between the 9 Ma initially prescribed load surface and the enhanced proximal sedimentation load surface is revealed by comparing the 2 and 3 km load contours of Fig. 11(A) to those in Fig. 11(B) (black heavy lines on left side). Near 30°S (~400 km north of the origin in our modelling domain), the initially prescribed load configuration has a very gentle slope (~1°) from medial to proximal Bermejo basin areas, and a very steep slope (~25°) from the proximal basin to the Central Precordillera (left side, Fig. 11A). At the same latitude, the enhanced proximal sedimentation load surface has a uniform slope (~4–5°) from the medial Bermejo basin to the Central Precordillera (left side, Fig. 11B). Both load surfaces involve the same crustal thickening due to sediment accumulation in the medial Bermejo basin near 30°S (H, left side Fig. 11A,B), but an additional sedimentary volume equivalent to the eroded 20–9 Ma strata

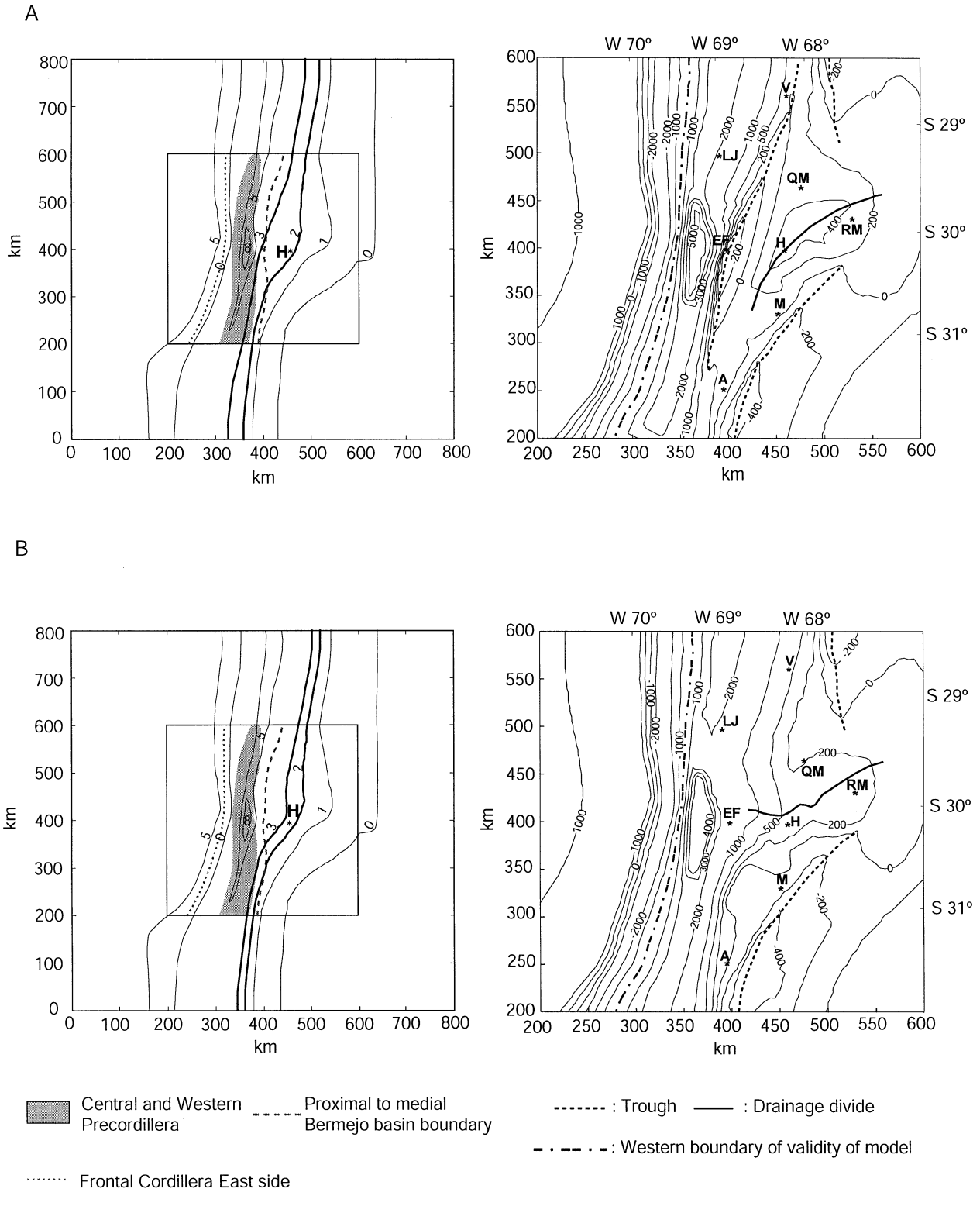

Fig. 11. The solution in three dimensions of loading of an homogeneous infinite elastic plate. On the left in each pair is the input 9 Ma load and on the right side is the resultant topography surface. (A) Three-dimensional load surface from interpolation of crustal loads prescribed in Fig. 6(A), (B) enhanced proximal sedimentation. In load surfaces (left side) the inside square denotes the area of interest in which the relative topography surfaces are displayed. Contours of the load in kilometres. In topography surfaces (right side) asterisks and capital letters denote the 9 Ma restored location of key columnar sections (see Fig. 2). Dash-dotted line marks what we conclude to be the western boundary of validity of our elastic model. Dashed and continuous thick lines denote troughs and divides, respectively. Contours in metres indicate topography, with a contour interval of 1000 m in the Precordillera and Cordillera Frontal, and 200 m in the Bermejo basin. The latitude/longitude grid (top and right margins) is a framework for comparison with Figs 2 and 3. The grid on the left and bottom margins are distance from the origin of the model. In all cases the thickness of the elastic lithosphere ($E=70$ GPa, $\nu=0.25$) is 30 km.

is considered in the enhanced proximal sedimentation load surface. These load configurations were tested on an elastic lithosphere of 20, 30, 40 or 50 km. The overall configuration of the resultant topography surfaces hardly varied in the four elastic thickness cases. As predicted in the 2D modelling, the flexural deformation field produced by the 20–9 Ma crustal loads is barely modified by uniformly weakening or stiffening the underlying lithosphere. Although we only show results for a constant elastic thickness lithosphere of 30 km (Fig. 11, right side), our observations apply equally well to elastic thicknesses ranging from 20 to 50 km.

The 9 Ma modelled topography surfaces (relative to an initially horizontal datum, right side, Fig. 11) clearly map the features predicted in our 2D simulations. An unrealistically large Iglesia–Calingasta depression (~2 km) west of 69°W marks the western limit of validity of our mechanical simulations (dash and dotted line in Fig. 11); west of it flexural deformation does not explain the inferred 9 Ma palaeotopography. The 9 Ma initially prescribed load surface produces a topography (Fig. 11A) with a steep, unrealistic slope (~10° at 30°S) at the most proximal Bermejo basin, a long proximal depression in the Bermejo basin (western trough, Fig. 11A), and a well-developed north-east trending forebulge in the medial basin (divide, Fig. 11A). The modelled topography resembles the 9 Ma palaeotopography near 31°S (south-eastern trough, Fig. 11A), but to the north the drainage that would form on the modelled topography would not only flow opposite to the geologically constrained drainage, but also unrealistically along strike towards a localized depression near the Río Jáchal (western trough, Fig. 11A). The 9 Ma enhanced proximal sedimentation load surface generates a relative topography (Fig. 11B) with a realistic, eastward-sloping depositional surface in the proximal Bermejo basin (~2° at 29°S, ~0.5° at 30°S, and ~3° at 31°S), and near the Río San Juan a topographic low that fits the 9 Ma palaeotopography (south-eastern trough, Fig. 11B). However, a forebulge in the medial Bermejo basin is still present, albeit less pronounced (divide, Fig. 11B).

An important result of our 2D and 3D analytical implementations is that flexural deformation of an elastic lithosphere due to a realistic, geologically constrained load configuration adjusted only for post 9 Ma erosion of proximal strata, explains the 9 Ma palaeotopography and along-strike variability of the strata in the proximal Bermejo basin. We cannot extend this conclusion to the medial Bermejo basin, where a prominent forebulge, a flexural response of the particular Precordillera crustal thickening configuration, prevails in all the simulations.

Variable elastic thickness lithosphere

The mountain belt–Bermejo basin system developed on a complex basement with inherited heterogeneities (Ramos *et al*., 1986). The 20–9 Ma Bermejo basin overlay a basement that consisted of two discrete terranes, the Famatina and Cuyania terranes (Ramos *et al*., 1986), delimited by the Valle Fértil lineament, which is today an east-dipping reverse fault (Figs 1A,B and 2B). To what extent these heterogeneities affected the strength (i.e. elastic thickness) of the lithosphere underlying the Bermejo basin is an interesting question. Our strategy is to evaluate the consequences of spatial variability of lithospheric strength (possibly related to the terranes) on tectonic subsidence in the Bermejo basin, using a 3D finite element model under the preferred 9 Ma load condition, with enhanced proximal sedimentation (left side, Fig. 11B).

Our simplest approximation of variable lithospheric strength geometry is a lithosphere with an elastic thickness that increases linearly to the east, from 5 km in the Frontal Cordillera and Iglesia–Calingasta basin to 50 km in the distal Bermejo basin (Fig. 12A). This elastic thickness geometry resembles the estimated present elastic thickness of the Andes–Bermejo basin lithosphere from 2D flexural modelling of regional gravity data (Stewart & Watts, 1997, their fig. 9, profiles 56 and 58). The resulting 9 Ma topography (Fig. 12A) exhibits a more pronounced east–west orientated divide in the medial Bermejo basin (compare Figs 11B—12A and 3E) and no other notable differences from the model with constant strength. Clearly, flexural deformation of a lithosphere with an elastic thickness linearly increasing to the east does not explain the 9 Ma palaeotopography of the Bermejo basin.

Along-strike changes in the thickness of the 20–9 Ma Bermejo basin strata (Fig. 2) suggest that the underlying lithosphere might change in rigidity along strike of the Precordillera and the proximal Bermejo basin (Jordan *et al*., 2001; Fig. 12B). Flexural deformation of a lithosphere with elastic thickness increasing to the east but low strength in the northern Precordillera (Fig. 12B) results in a slightly improved 9 Ma relative topography. The result contains an interrupted, less pronounced divide in the medial basin near 30°S, and more continuous topographic lows near 31°S and 29°S (Fig. 12B) compared to the constant elastic thickness case (Fig. 11B). The northern topographic low does not fit the inferred 9 Ma location of the Bermejo basin's axis (Figs 3E and 12B, see locality V), but at this latitude there are few geological constraints.

The next two test cases focus on the possible role of the Valle Fértil lineament and terrane boundary as a control on lithospheric strength. In the first case, we postulate that the strength of the lithosphere decreases linearly from the Central Precordillera to the Valle Fértil lineament, and remains constant east of there (Fig. 12C). The resultant 9 Ma relative topography (Fig. 12C) displays an interrupted divide in the medial Bermejo basin, and a south-eastern divide almost coincident with the 9 Ma restored position of the Pie de Palo basement uplift (Figs 12C, 1A and 2). The last feature is

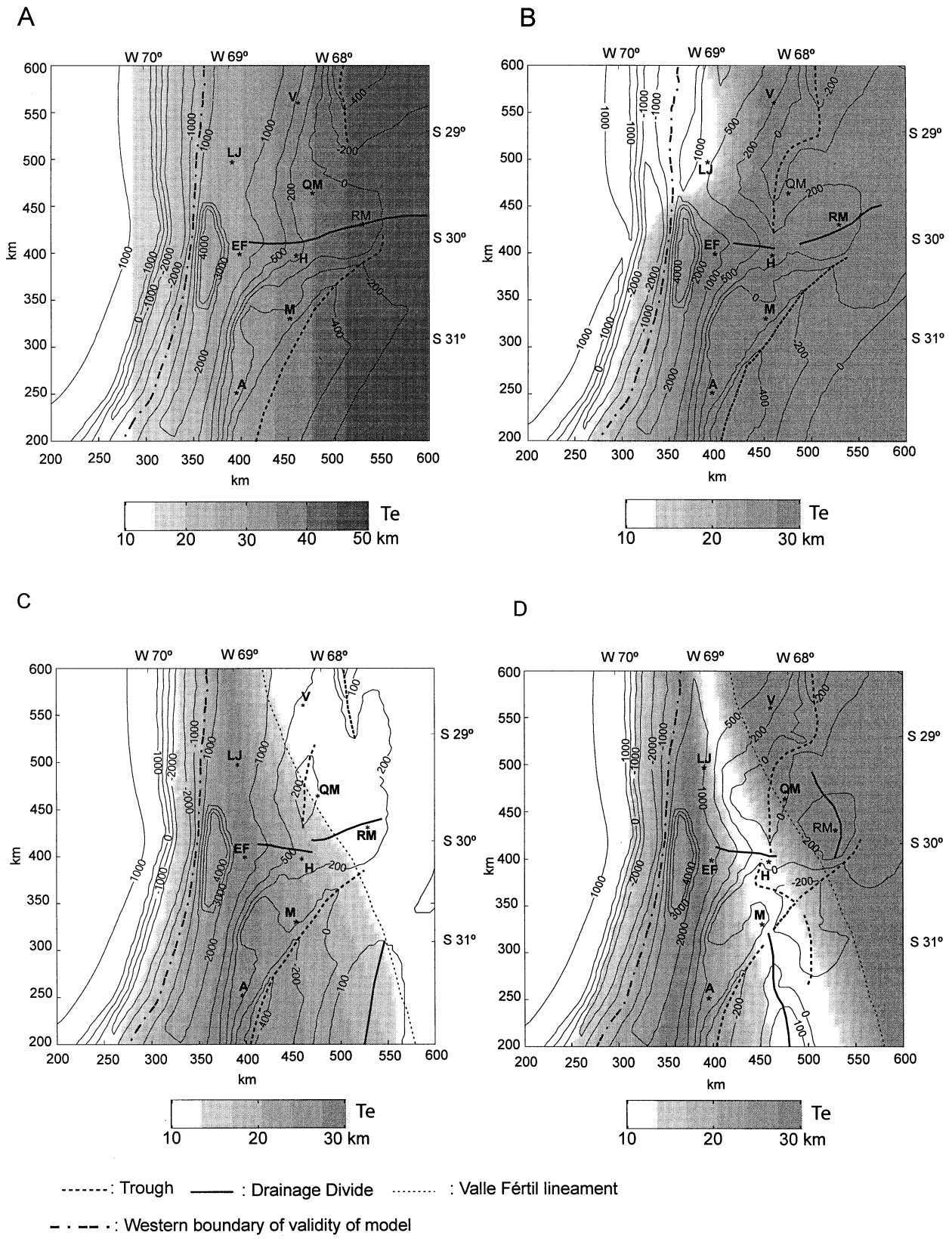

Fig. 12. Results of finite element models exploring lateral variability in thickness of the elastic lithosphere ($E=70$ GPa, $\nu=0.25$). The input loads are the same as in Fig. 11(B). (A) to (D) show the resultant relative topography at 9 Ma for (A) an eastward linear increase in rigidity, (B) a northern Precordillera low rigidity superimposed on an eastward linear increase in rigidity, (C) an eastward decrease in rigidity aligned with the Valle Fértil lineament (VF), and (D) a rigidity low along the Bermejo basin, parallel to VF. Light and dark grey denote weak and strong lithosphere, respectively. Contours in metres indicate topography, with a contour interval of 1000 m in the Precordillera and Cordillera Frontal, and 200 m in the Bermejo basin. Additional symbols and grids as in Fig. 11.

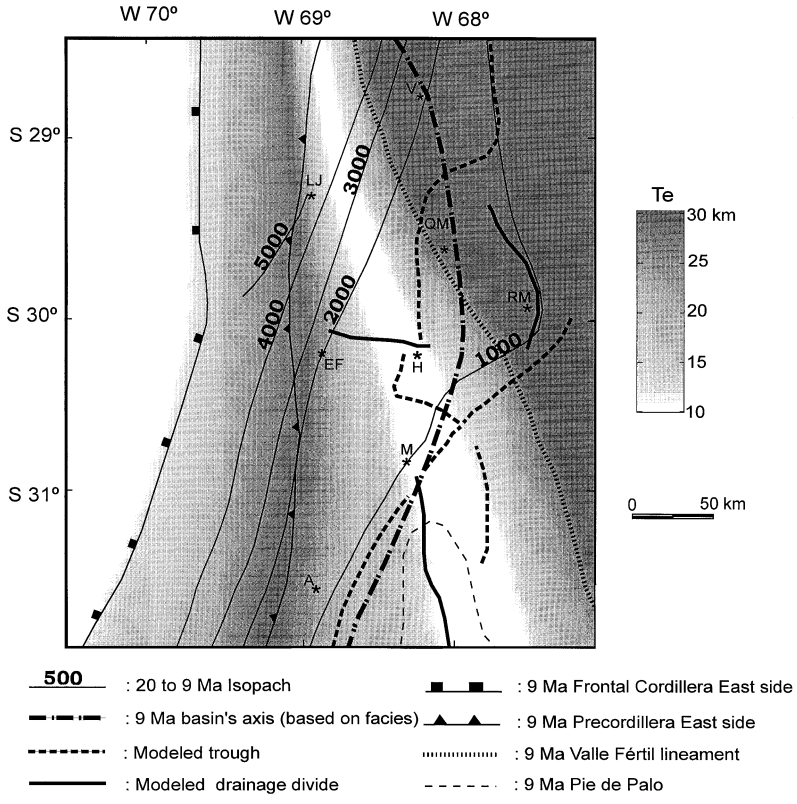

Fig. 13. The mechanical state of the Bermejo basin at 9 Ma. Grey tones indicate the strength of the lithosphere (T_e) underlying the Bermejo basin, dark for strong and light for weak lithosphere. Superimposed are: contours in metres of 20–9 Ma preserved strata (Fig. 2B), the restored 9 Ma basin axis or topographic low from facies patterns (Fig. 3E), the modelled troughs and divides in the 9 Ma relative topography of our preferred mechanical model (Fig. 12D), and the restored 9 Ma location of the east borders of the Frontal Cordillera and Central Precordillera, the Valle Fértil lineament, and Pie de Palo. The asterisks and capital letters indicate the 9 Ma restored location of key columnar sections (see Fig. 2). The latitude/longitude grid is a framework for comparison with Figs 2 and 3.

mandatory in any successful mechanical implementation, since the 20–9 Ma Bermejo basin isopach map shows a consistent decrease in accommodation space towards the Pie de Palo area (Fig. 2A,B).

The second alternative involving the Valle Fértil lineament is that the lithosphere weakens from the Central Precordillera to the axis of the Bermejo basin, where the strength is the minimum, and stiffens from the axis of the Bermejo basin to the Valle Fértil lineament, east of which the strength is constant. Such a strength field would resemble today's elastic thickness field derived from three-dimensional gravity data (Martinez & Introcaso, 1999; Ruiz & Introcaso, 1999). Figure 12(D) shows our preferred lithospheric rigidity geometry: an elastic lithosphere with the minimum strength in the Bermejo basin and Frontal Cordillera, and the maximum strength in the Central Precordillera and areas east of the Valle Fértil lineament. The modelled topography surface (Fig. 12D) resembles remarkably well the 9 Ma palaeotopography (Fig. 3E): a slightly interrupted topographic low runs along the basin (see northern and southern troughs, Fig. 12D). The east-trending divide in the medial Bermejo basin is not present, and instead there are two higher areas in the Eastern to Central Precordillera (EF, Figs 12D and 13) and near Río Mañero (RM, Figs 12D and 13). From near 31°S southward, a NNW-trending divide with a relative relief of 300 m coincides with the Pie de Palo restored location (east of U, Figs 12D and 13). In a fashion similar to the real 9 Ma Bermejo basin, the distance from the deforming orogen to the modelled forebulge narrows southward, from about 200 km near 29°S to less than 100 km near 31°S (Figs 12D and 13). We interpret that the triangular area of weak lithosphere below the Bermejo basin results from either an unusual composition of the crust and mantle lithosphere compared to neighbouring terranes, or modification of the crust and mantle lithosphere by the terrane assembly processes. The result is a southward decrease in wavelength of the flexural deformation induced by the Precordillera thrust system.

DISCUSSION

Tectonic subsidence in the 20–9 Ma Bermejo basin is well approximated by flexural deformation of an homogeneous, isotropic, linear, and elastic lithosphere. Because the 20–9 Ma crustal loads and lithospheric strength were variable in space, the basin's cross-sectional geometry departed from an 'ideal' sedimentary wedge (Flemings & Jordan, 1990). However, flexural compensation of crustal loads did not operate west of the Precordillera thrust belt. Rather, the failure of our 2D and 3D models to replicate the 9 Ma topography in the Iglesia–Calingasta basin suggests that local isostatic compensation prevailed there and in the high Andes to its west. Today also, the crustal loads remain locally compensated west of the Precordillera thrust belt, as supported by regional gravity data (Stewart & Watts, 1997).

Our constant elastic thickness (e.g. strength) models illustrated that the magnitudes and wavelengths of the modelled topographic highs and lows in the Precordillera and Bermejo basin were plausible, and therefore we concluded that an elastic rheology was probably a good

mechanical approximation. But those models also show a lack of importance of the Frontal Cordillera in the mechanical system of the Bermejo basin, except as a source of sedimentary loads, and the need for minor adjustments to the geologically preserved record of crustal loads. The 9 Ma basin axis, or topographic low, and the southward narrowing of the basin cannot be replicated with a constant elastic thickness lithosphere. A finite element model of a lithosphere with spatially variable elastic thickness proved much more effective in explaining tectonic subsidence in the basin (Figs 12D and 13). Flexural deformation of an elastic lithosphere with low strength below the Bermejo basin and west of the Precordillera, and higher strength below the Precordillera and areas east of the Valle Fértil lineament, resulted in a predicted topography configuration that was remarkably similar to the 9 Ma basin palaeotopography, including a basin that narrowed southward as does the 9 Ma Bermejo basin (Fig. 13).

Spatially variable crustal loading and lithospheric strength equally influence the stratigraphy of the 20–9 Ma Bermejo basin. An interesting observation is that the preferred 9 Ma lithospheric strength distribution is similar to the present lithospheric strength geometry, estimated from flexural modelling of gravity data (Gimenez, 1997; Martinez & Introcaso, 1999; Ruiz & Introcaso, 1999). A lithosphere with a bimodal strength distribution seems to prevail during the entire Bermejo basin evolution. This implies that the inherited strength of the lithosphere underlying the Bermejo basin is preserved for at least 20 Myr (e.g. Watts, 1992). Contrary to the predictions of Lavier & Steckler (1997), the ~8–10 km sedimentary cover of the Bermejo basin (which existed by the end of the Pliocene but not at 20 Ma) had no apparent effect on the strength of the underlying lithosphere.

The recognition that the lithosphere underlying the Bermejo basin was weak during an early part of the basin's evolution diminishes the need to think that the flattening of the subducting slab and the tectonic change to a broken foreland (Jordan & Allmendinger, 1986; Kay *et al*., 1988) weakened the plate to the state now revealed in the gravity data. The long-term lithospheric weakness and the high-amplitude, short-wavelength flexural response of the lithosphere underlying the Bermejo basin help to explain why the thickness and accumulation rates in the basin exceed those of most other retroarc foreland basins (e.g. Jordan, 1995). Considering how weak the lithosphere underlying the Bermejo basin is, how thick the Precordillera load is, and how arid (slow denudation) the area is, one might expect the basin to have subsided below sea level. The fact that the preserved Bermejo strata are all continental implies that the pre-20 Ma basin elevation was considerably above sea level, perhaps because the Bermejo crustal thickness was initially greater than previously thought (e.g. estimated to have been ~33 km in the Eastern Precordillera; Zapata, 1998).

Maggi *et al*. (2000) proposed that there exists a correlation in Eurasia between the strength distribution measured by elastic thickness of the lithosphere (defined by gravity anomalies and topography) and the thickness of the seismogenic crust. Our result appears inconsistent with Maggi *et al*.'s (2000) hypothesis. The sector of the Bermejo basin for which hypocentral locations of earthquakes are well known (south of 31°S) features middle and upper crustal earthquakes in an unusually thick seismogenic zone of relatively uniform thickness (30 km beneath Pie de Palo and 35 km beneath the Central and Eastern Precordillera) (Smalley & Isacks, 1990; Regnier *et al*., 1992; Smalley *et al*., 1993). But our modelling results imply that the elastic thickness increases markedly from east to west (5–10 km beneath Pie de Palo to 25 km beneath what is now the Central Precordillera) (Fig. 13). The inconsistency is focused on the conflicting indications for Pie de Palo and the flanking Bermejo basin, where merely 5–10 km of the lithosphere was sufficiently strong to behave as an elastic plate, but as much as 32 km of the crust is strong enough to generate earthquakes. If the evidence of a weak elastic plate proves to be confined to a time some 10 million years ago (our model), one may be able to explain the discrepancy as the result of transient conditions (e.g. delamination prior to flattening of the Nazca plate that could have made the region weak, or unusually high stress applied to the crust today; Smalley & Isacks, 1990). Whether or not the same pattern of lithospheric strength exists today is uncertain, because only north of 31°S has a dense grid of gravity data been modelled (Giménez, 1997; Martinez & Introcaso, 1999; Ruiz & Introcaso, 1999). Those gravity studies demonstrate that the Bermejo valley lithosphere is weak today, whereas the region east of the Valle Fértil lineament is strong. Although several studies of regional gravity data reached the conclusion that the Precordillera itself is also weak (Introcaso *et al*., 1992; Tassara & Yañez, 1996), the gravity data have not been studied at a sufficient spatial resolution to test a short-wavelength variation in strength between the Bermejo valley, Pie de Palo, and the Precordillera. Pending more studies, the seeming discrepancy between a thick strong zone implied by seismic activity and thin (or absent) strong zone implied by the stratigraphic modelling remains an enigma.

ACKNOWLEDGMENTS

We thank Richard Allmendinger, Elías Gómez, Ernesto Cristallini, and Matt Burns for numerous constructive discussions. Kanwaljeet Bawa-Bhalla provided invaluable assistance with the finite element simulations. YPF S.A. generously permitted use of their seismic data. Critical reviews of this paper by Fritz Schlunegger and

Peter Burgess are greatly appreciated. Supported by grant EAR-9614286 from the U.S. National Science Foundation.

REFERENCES

Allmendinger, R.W., Figueroa, D., Snyder, D., Beer, J., Mpodozis, C. & Isacks, B.L. (1990) Foreland shortening and crustal balancing in the Andes at 30°S Latitude. *Tectonics*, **9,** 789–809.

Astini, R.A. (1991) *Paleoambientes sedimentarios y secuencias depositacionales del Ordovicico clastico de la Precordillera Argentina*. PhD Thesis, Universidad Nacional de Cordoba.

Baraldo, J.A. (1985) Estructura de un sector de la Precordillera nororiental Sanjuanina, Dpto, Jáchal, San Juan. *Primeras Jornadas Sobre Geologia Precordillera*, Acta I, 209–214.

Beaumont, C. (1981) Foreland basins. *Geophys. J. Royal Astronom. Soc.*, **65,** 291–329.

Beer, J.A. (1990) Steady sedimentation and lithologic completeness, Bermejo basin, Argentina. *J. Geol.*, **98,** 501–518.

Beer, J.A., Allmendinger, R.W., Figueroa, D.E. & Jordan, T.E. (1990) Seismic stratigraphy of a Neogene Piggyback Basin, Argentina. *AAPG Bull.*, **74,** 1183–1202.

Beer, J.A. & Jordan, T.E. (1989) The effects of Neogene thrusting on deposition in the Bermejo Basin, Argentina. *J. Sedimen. Petrol.*, **59,** 330–345.

Bercowski, F., Berenstein, L.R. & Johnson, N.M. (1987) Litofacies y paleoambiente del Terciario en Loma de Las Tapias, Ullum, Provincia de San Juan, Argentina. *X Congreso Geológico Argentino, Tucumán*, **2,** 101–104.

Bercowski, F., Berenstein, L.R., Johnson, N.M. & Naeser, C.W. (1986) Sedimentología, magnetoestratigrafía y edad isotópica del Terciario en Loma de las Tapias, Ullum, Provincia de San Juan. *Primera Reunión Sedimentológica Argentina, Plata*, Actas, 169–172.

Bercowski, F. & Figueroa, G.J. (1989) Depósitos piroclastásticos en la Formación Albarracín, Terciario, Precordillera Sanjuanina. *Asociación Geo. Argentina, Revista*, **43,** 28–34.

Bercowski, F., Jordan, T.E., Zeitler, P., Caballero, M.M., Pérez, I. & Carrizo, C. (1994) Correlaciones estratigráficas en el neozoico de Precordillera central, San Juan, Argentina. *7th Congreso Geológico Chileno*, **1,** 404–408.

Brooks, B.A. (1999) *Fault spacing in the El Teniente Mine, central Chile; the fold style inversion method; fold segmentation and fault linkage of the Barrancas/Lunlunta-Carrizal anticlinal complex, Mendoza, Argentina*. Cornell University, Ithaca, NY, USA.

Caminos, R., Fauque, L., Cingolani, C., Varela, R. & Morel, E. (1993) Estratigrafía y estructura del Devonico-Carbonifero en el sector septentrional de la Sierra de la Punilla, Precordillera de La Rioja y San Juan. *XII Congreso Geológico Argentino Y II Congreso Exploración Hidrocarburos*, **2,** 31–41.

Cevallos, M. & Milana, J.P. (1992) Sedimentología de un desierto eólico terciario (San Juan, Argentine). *IV Reunión Argentina Sedmentología*, **3,** 121–128.

Clark, M.K. & Royden, L.H. (2000) Topographic ooze; building the eastern margin of Tibet by lower crustal flow. *Geology*, **28,** 703–706.

Coughlin, T.J., O'Sullivan, P.B., Kohn, B.P. & Holcombe, R.J. (1998) Apatite fission-track thermochronology of the Sierras Pampeanas, central western Argentina: Implications for the mechanism of plateau uplift in the Andes. *Geology*, **26,** 999–1002.

Cristallini, E.O. & Ramos, V.A. (2000) Thick-skinned and thin-skinned thrusting in the La Ramada fold and thrust belt: crustal evolution of the High Andes of San Juan, Argentina (32°SL). *Tectonophysics*, **317,** 205–235.

Damanti, J.F. (1989) Evolution of the Bermejo foreland basin: provenance, drainage development diagenesis. Doctoral Thesis, Cornell University, Ithaca, NY, USA.

Damanti, J.F. & Jordan, T.E. (1989) Cementation and Compaction History of Synorogenic Foreland Basin Sedimentary Rocks from Huaco, Argentina. *AAPG Bull.*, **73,** 858–873.

Decelles, P.G. & Mitra, G. (1995) History of the Sevier orogenic wedge in terms of critical taper models, northeast Utah and southwest Wyoming. *GSA Bull.*, **107,** 454–462.

Fernández, A.E. (1996) Seismic analysis, paleoclimatology and fluvial architecture of the Bermejo Basin, Central Andes, Western Argentina. Doctoral Thesis, Cornell University, Ithaca, NY, USA.

Fernández, A.E. & Jordan, T.E. (1996) Analysis of controls on foreland basin stratigraphy using seismic and outcrop data: application to the Bermejo basin, central Andes, Argentina. *XIII Congreso Geológico Argentino III Congreso Exploración Hidrocarburos, Buenos Aires*, **1,** 373–384.

Fernández-Seveso, F., Perez, M.A., Brisson, I.E. & Alvarez, L. (1993) Sequence stratigraphy and tectonic analyisis of the Paganzo basin, Western Argentina. *Comptens Rendus XII ICC-P*, **2,** 223–260.

Flemings, P.B. & Jordan, T.E. (1989) A synthetic stratigraphic model of foreland basin development. *J. Geophys. Res.*, **94,** B3851–B3866.

Flemings, P.B. & Jordan, T.E. (1990) Stratigraphic modelling of foreland basins: interpreting thrust deformation and lithospheric rheology. *Geology*, **18,** 430–435.

Flemings, P.B. & Nelson, S.N. (1991) Paleogeographic evolution of the latest Cretaceous and Paleocene Wind River basin. *Mountain Geologist*, **28,** 37–52.

Furque, G. (1963) *Hoja 17b-Guandacol*. Direccion de Geologia y Mineria, Argentina.

Giménez, M.E. (1997) *Estudio genético y evolutivo de la Cuenca del Bermejo (Provincia de San Juan), a partir de datos de gravedad*. Doctoral Thesis, Universidad Nacional de Rosario, Rosario, Santa Fe, Argentina.

von Gosen, W. (1992) Structural evolution of the Argentine Precordillera: the Río San juan section. *J. Struct. Geol.*, **14,** 643–667.

von Gosen, W. (1995) Polyphase structural evolution of the southwestern Argentine Precordillera. *J. South Am. Earth Sci.*, **8,** 377–404.

von Gosen, W. (1997) Early Paleozoic and Andean structural evolution in the Río Jáchal section of the Argentine Precordillera. *J. South Am. Earth Sci.*, **10,** 361–388.

Hetényi, M. (1946) *Beams on Elastic Foundations. Theory with Applications in the Fields of Civil and Mechanical Engineering*. The University of Michigan Press.

Horton, B.K. (1999) Erosional control on thrust belt development in the Bolivian Andes. *Fourth International Symposium on Andean Geodynamics, Göttingen*, 334.

Huebner, K.H., Thornton, E.A. & Byrom, T.G. (1995) *The Finite Element Method for Engineers*. John Wiley & Sons, Inc.

Introcaso, A., Pacino, M.G. & Fraga, H. (1992) Gravity, isostasy, and Andean crustal shortening between latitudes 30° and 35°S. *Tectonophysics*, **205,** 31–48.

Johnson, N.M., Jordan, T.E., Johnsson, P.A. & Naeser, C.W. (1986) Magnetic polarity stratigraphy, age and tectonic setting of fluvial sediments in the eastern Andean foreland basin, San Juan province, Argentina. In: Foreland Basins (Ed. by P.A. Allen & P. Homewood), *Int. Ass. Sedimentol., Spec. Publ.*, **8,** 63–75.

Johnsson, P.A., Johnson, N.M., Jordan, T.E. & Naeser, C.W. (1984) Magnetic polarity stratigraphy and age of the Quebrada del Cura, Río Jáchal, and Mogna Formations near Huaco, San Juan Province, Argentina. *IX Congreso Geologico Argentino*, **3,** 81–96.

Jordan, T.E. (1981) Thrust loads and foreland basin evolution, Cretaceous, western United States. *AAPG Bull.*, **65,** 2506–2520.

Jordan, T.E. (1995) Retroarc Foreland and Related Basins. In: *Tectonics of Sedimentary Basins* (Ed. by C. Busby & R. Ingersoll), pp. 331–362. Blackwell Scientific Publications, Oxford.

Jordan, T.E. & Allmendinger, R.W. (1986) The Sierra Pampeanas of Argentina: a modern analogue of Rocky Mountain foreland deformation. *Am. J. Sci.*, **286,** 737–764.

Jordan, T.E., Allmendinger, R.W., Damanti, J.F. & Drake, R.E. (1993a) Chronology of Motion in a Complete Thrust Belt: the Precordillera. 30–31°S, Andes Mountains. *J. Geol.*, **101,** 135–156.

Jordan, T.E., Drake, R.E. & Naeser, C.W. (1993b) Estratigrafía del cenozoico medio en la Precordillera a la latitud del Río Jáchal, San Juán, Argentina. *XII Congreso Geológico Argentino Y II Congreso Exploración Hidrocarburos*, **2,** 132–141.

Jordan, T.E., Kelley, S., Fernández, A., Ferrnández Seveso, F., Ré, G. & Milana, J.P. (1997) Relaciones entre las historias evolutivas de las cuencas de Iglesia y Bermejo, Provincia de San Juan. *Argentina. II Jornadas Geología Precordillera, San Juan, Argentina*, 142–147.

Jordan, T.E., Rutty, P.M., McRae, L.E., Beer, J.A., Tabbutt, K. & Damanti, J.F. (1990) Magnetic polarity stratigraphy of the Miocene Río Azul section, Precordillera thrust belt, San Juan Province, Argentina. *J. Geol.*, **98,** 519–539.

Jordan, T.E., Schlunegger, F. & Cardozo, N. (2001) Unsteady and Spatially Variable Evolution of the Neogene Andean Bermejo Foreland Basin, Argentina. *J. South Am. Earth Sci.*, in press.

Kay, S.M., Maksaev, V., Moscoso, R., Mpodozis, C., Nasi, C. & Gordillo, C.E. (1988) Tertiary Andean mamatism in Chile and Argentina between 28°S and 33°S: correlation of magmatic chemistry with a changing Benioff zone. *J. South Am. Earth Sci.*, **1,** 21–38.

Lavier, L.L. & Steckler, M.S. (1997) The effect of sedimentary cover on the flexural strength of continental lithosphere. *Nature*, **389,** 476–479.

Maggi, A., Jackson, J.A., McKenzie, D. & Priestley, K. (2000) Earthquake focal depths, effective elastic thickness, and the strength of the continental lithosphere. *Geology*, **28,** 495–498.

Malizia, D.C., Reynolds, J.H. & Tabbutt, K.D. (1995) Chronology of Neogene sedimentation, stratigraphy, and tectonism in the Campo de Talampaya region, La Rioja Province, Argentina. *Sediment. Geol.*, **96,** 231–255.

Malizzia, D.C. & Limeres, M.H. (1984) Estudio de facies de la Formación Quebrada del Médano en el perfil de la quebrada eponima, Provincia de La Rioja. *IX Congreso Geológico Argentina (Bariloche)*, **1,** 310–321.

Martinez, M.P. & Introcaso, A. (1999) *La Sierra Pampeana de Valle Fértil, Provincia de San Juan. Análisis Estructural a partir de Datos Gravimétricos*. UNR Editora, Universidad Nacional de Rosario.

Milana, J.P. (1990a) Facies y paleohidrología de conglomerados aluviales Plio-Pleistocenos (San Juan, Argentina): evidencias de fases climáticas en los Andes a los 31°Sur. *Segundo Simposio sobre el. Terciario Chile (Concepción)*, 215–224.

Milana, J.P. (1990b) Secuencias sedimentarias aluviales, subsidence y tectonismo en la cuenca de antepaís andina de la provincia de San Juan, Argentina. *Segundo Simposio Sobre El Terciario Chile (Concepción)*, 205–214.

Milana, J.P. (1991) *Sedimentología y magnetoestratigrafía de formaciones cenozoicas en el area de Mogna y su inserción en el marco tectosedimentario de la Precordillera Oriental*. Universidad Nacional de San Juan, Argentina.

Milana, J.P. (1993) Estratigrafía de eólianitas en la zona de Jáchal–Huaco, Precordillera de San Juan. *Asociación Geológica Argentina, Revista*, **48,** 283–298.

Milana, J.P., Cevallos, M.F., Zavattieri, A.M., Prampano, M. & Papu, H.O. (1993) La secuencia terciaria de Pachaco: sedimentología, edad, correlaciones y significado paleo-geográfico. *XII Congreso Geológico Argentino Y II Congreso Exploración Hidrocarburos*, **1,** 226–234.

Parker, G. (1974) Posición estratigráfica del 'Famatinense' y sus correlaciones. *Revista Asociación Geológica Argentina*, **29,** 231–247.

Ramos, V.A. (1970) Estratigrafía y estructura del Terciario en la Sierra de los Colorados (Provincia de La Rioja), República Argentina. *Asociación Geológica Argentina, Revista*, **25,** 359–382.

Ramos, V.A., Cegarra, M., Lo Forte, G. & Cominguez, A. (1997) El frente orogénico en la Sierra de Pedernal (San Juan, Argentina): su migración a través de los depósitos sinorogénicos. *VIII Congreso Geológico Chileno*, **3,** 170–1713.

Ramos, V.A. & Cristallini, E. (1995) Perfil estructural de la Precordillera a lo largo del Río San Juan. *Andean Thrust Tectonics Symposium, Field Guide*, San Juan, Argentina. pp. 1–42.

Ramos, V.A., Jordan, T.E., Allmendginer, R.W., Mpodozis, C., Kay, S.M., Cortés, J.M. & Palma, M. (1986) Paleozoic terranes of the Central Argentine-Chilean Andes. *Tectonics*, **5,** 855–880.

Re, G.H. (1995) Evolución tectosedimentaria del depocentro de la Cuenca del Antepaís Andino (27° a 33°) y relación con el cambio en el ángulo de subducción de la Placa de Nazca. *IX Congreso Latinoamericano de Geología*. Ministerio de Energía y Minas, Caracas, Venezuela (published as a CD).

Re, G.H. (1998) Magnetoestratigrafía y tasa de sedimentación de la Formación Toro Negro (Sierra de los Colorado, La Rioja). *X Congreso Latinoamericano Geología Y VI Congreso Nacional Geología Económica*, **1,** 162.

Re, G.H. & Vilas, J.F. (1990) Análisis de los cambios paleogeográficos ocurridos durante el Cenozoico tardío en la región de Vinchina (Provincia de La Rioja, Argentina), a partir de estudios magnetoestratigráficos. *XI Congreso Geológico Argentina*, **2,** 267–270.

Regnier, M., Chatelain, J.L., Smalley, R., Chiu, J.M., Isacks, B.L. & Araujo, M. (1992) Seismotectonics of Sierra Pie de Palo, a basement block uplift in the Andean foreland of Argentina. *Bull. Seismol. Soc. Am.*, **82,** 2549–2571.

Reynolds, J.H., Jordan, T.E., Johnson, N.M. & Tabbutt, K.D. (1990) Neogene deformation of the flat-subduction segment of the Argentine-Chilean Andes: Chronological constraints from Las Juntas, Argentina. *GSA Bull.*, **102,** 1607–1622.

Rodríguez Fernández, L.R., Heredia, N., Marín, G., Quesada, C., Robador, A., Ragona, D. & Cardó, R. (1996) Tectonoestratigrafía y Estructura de los Andes Argentinos entre los 30°30′ y 31°00′ de latitud S. *XIII Congreso Geológico Argentino Y III Congreso Exploración Hidrocarburos*, **2,** 111–124.

Ruiz, F. & Introcaso, A. (1999) Resultados gravi-magnetométricos sobre una sección que atravieza en 29°30′S a la cuenca Ischigualasto-Villa Unión (San Juan y La Rioja). *XIV Congreso Geológico Argentino. Actas I, Salta*, 306–309.

Salfity, J. & Gorustovich, S. (1983) Paleogeografía de la Cuenca del Grupo Paganzo (Paleozoico superior). *Rev. Asoc. Geol. Argentina*, **38,** 437–453.

Schlunegger, F. (1999) Controls of surface erosion of the Alps: constraints from the stratigraphies of the adjacent foreland basins. *Int. J. Earth Sci.*, **88,** 285–304.

Schlunegger, F., Jordan, T.E. & Klaper, E.M. (1997) Controls of erosional denudation in the orogen on foreland basin evolution; the Oligocene central Swiss Molasse Basin as an example. *Tectonics*, **16,** 823–840.

Sclater, J.G. & Christie, P.A.F. (1980) Continental stretching: an explanation of the post-mid-Cretaceous subsidence of the central North Sea basin. *J. Geophys. Res.*, **85,** 3711–3739.

Smalley, R. & Isacks, B.L. (1990) Seismotectonics of thin- and thick-Skinned deformation in the Andean Foreland from local network data: Evidence for a seismogenic lower crust. *J. Geophys. Res.*, **95,** 12487–12498.

Smalley, R., Pujol, J., Regnier, M., Chiu, J.M., Chatelain, J.L., Isacks, B.L., Araujo, M. & Puebla, N. (1993) Basement Seismicity beneath the Andean Precordillera thin-skninned thrust belt and implication for crustal and lithospheric behavior. *Tectonics*, **12,** 63–76.

Stewart, J. & Watts, A.B. (1997) Gravity anomalies and spatial variations of flexural rigidity at mountain ranges. *J. Geophys. Res.*, **102,** 5327–5352.

Stockmal, G.S. & Beaumont, C. (1987) Geodynamic models of convergent margin tectonics: The southern Canadial Cordillera and the Swiss Alps. *Can. Soc. Petrol. Geol. Mem.*, **12,** 393–411.

Tabbutt, K., Naeser, C.W., Jordan, T.E. & Cerveny, P.F. (1989) New fission-track ages of Mio-Pliocene tuffs in the Sierras Pampeanas and Precordillera of Argentina. *Asoc. Geol. Argentina, Revista*, **34,** 408–419.

Tassara, A. & Yañez, G. (1996) Thermomechanic segmentation of the Andes (15°–50°S): a flexural analysis approach. *Third ISAG (International Symposium of Andean Geodynamics)*, St Malo, France, pp. 17–19.

Timoshenko, S. & Woinowsky-Krieger, S. (1959) *Theory of Plates and Shells*, 2nd edn. McGraw-Hill.

Turcotte, D.L. & Schubert, G. (1982) *Geodynamics, Applications of Continuum Physics to Geological Problems*. John Wiley & Sons, New York.

Ugural, A.C. & Fenster, S.K. (1995) *Advanced Strength and Applied Elasticity*. Prentice Hall.

Watts, A.B. (1992) The effective elastic thickness of the lithosphere and the evolution of foreland basins. *Basin Res.*, **4,** 169–178.

Whiting, B.M. & Thomas, W.A. (1994) Three-dimensional controls on subsidence of a foreland basin associated with a thrust belt recess: Black Warrior basin, Alabama and Mississippi. *Geology*, **22,** 727–730.

Yañez, G.A., Canuta, J., Tassara, A. & Giavelli, A. (1995) Flexural analysis along the Southern Andes, between 12 degrees and 58 degrees S. *Int. Union Geodesy Geophysics; XXI General Assembly; Abstracts*, **21,** 429.

Zambrano, J., Sanchez, A. & Hernandez, M. (1996) Aspectos estratigraficos y estructurales del sector Gualcamayo-Guandacol (Provincia de La Rioja y San Juan-Argentina) relacionados con la exploracion minera metalifera. *XIII Congreso Geologico Argentino Y III Congreso Exploracion Hidrocarburos*, **1,** 531–540.

Zapata, T.R. (1996) *Crustal Evolution of the Precordillera Thrust Belt–Bermejo Basin, Argentina*. PhD Thesis, Cornell University, 243.

Zapata, T.R. (1998) Crustal structure of the Andean thrust front an 30°S latitude from shallow and deep seismic reflection profiles, Argentina. *J. South Am. Earth Sci.*, **11,** 131–151.

Zapata, T.R. & Allmendinger, R.W. (1996a) Growth stratal records of instantaneous and progressive limb rotation in the Precordillera thrust belt and Bermejo basin, Argentina. *Tectonics*, **15,** 1065–1083.

Zapata, T.R. & Allmendinger, R.W. (1996b) The thrust front zone of the Precordillera, Argentina: a thick-skinned triangle zone. *Am. Assoc. Petrol. Geol. Bull.*, **80,** 359–381.

Zienkiewicz, O.C. (1977) *The Finite Element Method*. McGraw-Hill.

Received 13 October 2000; revision accepted 14 May 2001